


國立交通大學

電子工程學系 電子研究所碩士班

碩士論文

應用於系統面板之連續波雷射結晶多晶矽薄膜

電晶體之研究



**Study on the Continuous Wave Laser
Crystallized Polycrystalline Silicon Thin-Film
Transistors for the System-on-Panel
Applications**

研究生：胡明哲

Ming-Jhe Hu

指導教授：鄭晃忠 博士

Dr. Huang-Chung Cheng

中華民國 九十九 年 八 月

應用於系統面板之連續波雷射結晶多晶矽薄膜電晶體之

研究

**Study on the Continuous Wave Laser Crystallized Polycrystalline
Silicon Thin-Film Transistors for the System-on-Panel Applications**

研 究 生：胡明哲

Student: Ming-Jhe Hu

指導教授：鄭晃忠 博士

Advisor: Dr. Huang-Chung Cheng

國立交通大學

電子工程學系 電子研究所碩士班

碩士論文

A Thesis

Submitted to Department of Electronics Engineering
& Institute of Electronics

College of Electrical & Computer Engineering

National Chiao Tung University

In Partial Fulfillment of the Requirements

for the degree of master

in

Electronics Engineering

August, 2010

Hsinchu, Taiwan, Republic of China

中華民國 九十九 年 八 月

應用於系統面板之連續波雷射結晶多晶矽薄膜電晶體 之研究

研究生：胡明哲

指導教授：鄭晃忠 博士

國立交通大學

電子工程學系 電子研究所碩士班

摘要

近來低溫多晶矽薄膜電晶體已被廣泛應用於主動式平面顯示器，其是因為低溫多晶矽薄膜電晶體具有高的載子遷移率、低功耗。況且可將周邊驅動電路和功能性電路整合至玻璃面板達成低製作成本、高可靠度與系統面板(System-on-Panel)的目標，在未來應用於三維積體電路(3-D ICs)的實現具有很大的潛力。

要達到絕緣層上矽元件(SOI)特性，本質上來說，可以藉由結晶非晶矽薄膜並增大多晶矽的晶粒大小，減少晶粒缺陷以趨近於單晶矽元件之特性。這些將非晶矽薄膜再結晶為多晶矽的技術包含固相結晶法(SPC)、金屬誘導結晶法(MIC)、準分子雷射結晶法(ELC)等。然而這些技術都有一些缺點，以固相結晶的多晶矽薄膜電晶體需要較長的結晶時間，且有較多的晶粒缺陷，因此導致較差的元件特性。而金屬誘導結晶的多晶矽薄膜，有金屬殘留的問題。在準分子雷射結晶法來說，此技術可有效增加晶粒大小，然而在超級側向成長(SLG)的製程能量區間範圍過窄，以及較差的晶粒大小均勻度是這個技術的主要缺點。因此，本論文主要

提出一種二極體泵浦固態 (DPSS) 連續波雷射結晶 (CLC) 技術，由於此技術可控制結晶機制為沿著雷射掃描方向之縱向成長 (Longitudinal Growth)，因此以此法結晶之多晶矽薄膜電晶體有較佳的載子遷移率。

本論文主要分成兩個部分，在第一部分，藉由控制雷射能量為 2.4 W 至 4.0 W 間與雷射掃描速度為 20 mm/s 至 60 mm/s，可以在雷射光束中間區域成長大型縱向成長的多晶矽晶粒。然而在雷射光束的邊緣區與過度區仍然有小晶粒與多邊形的晶粒存在，它們分別對應的成長機制為固相結晶型與部分融熔到類超級側向成長型。若多晶矽薄膜電晶體的多晶矽通道屬於小晶粒或多邊形的晶粒，將明顯地降低多晶矽薄膜電晶體的效能，而在雷射光束中間區域所成長的晶粒其機制是全熔融之液相沿著縱向固化的超大晶粒之成長方式。其次，我們也提出多次掃描的方式達成大面積縱向結晶成長，實驗結果顯示晶粒大小可達數十微米、表面粗糙度介於 13.308 nm 至 18.671 nm 以及好的結晶性。

在第二部分，我們研究了不同結晶機制下的連續波雷射結晶的多晶矽薄膜電晶體特性。在固相結晶區域，N 型多晶矽薄膜電晶體的載子遷移率、次臨界擺幅和臨界電壓，分別為 19.4 cm²/V-s、2.72 V/decade 和 7.93 V。在部分融熔到類超級側向成長區域，N 型多晶矽薄膜電晶體的載子遷移率、次臨界擺幅和臨界電壓，分別為 86.9 cm²/V-s、1.41 V/decade 和 0.296 V。在縱向結晶區間，較高效能的 N 型多晶矽薄膜電晶體的載子遷移率、次臨界擺幅和臨界電壓，分別可達到 281 cm²/V-s、0.753 V/decade 和 -1.17 V。這些結果顯示晶粒越大且結晶性越佳將有較佳之電性。因此，如此簡單的連續波雷射結晶科技對於在未來三維積體電路應用上其發展將是不容小懼的。

Study on the Continuous Wave Laser Crystallized Polycrystalline Silicon Thin-Film Transistors for the System-on-Panel Applications

Student: Ming-Jhe Hu

Advisor: Dr. Huang-Chung Cheng

**Department of Electronics Engineering & Institute of Electronics
National Chiao Tung University**



ABSTRACT

Low-temperature polycrystalline silicon (LTPS) thin film transistors (TFTs) have been widely used in active matrix flat panel displays (AMFPDs), since they feature in high field-effect mobility and low power consumption. Moreover, the peripheral driver circuits, controller ICs and functional circuits can be integrated into glass substrates by utilizing LTPS-TFTs to achieve the goal of low cost, high reliability and System-on-Panel (SOP). We can foresee that LTPS-TFTs have great potential in the realization of 3-D ICs in the near future.

In tradition, reducing the defect states via enlarging poly-Si grain size is an intrinsic approach to single crystal Si material, which leads to the silicon-on-insulator-like (SOI-like) device performance. There are several technologies to enlarge the grain size, including solid phase crystallization (SPC)

metal induced crystallization (MIC), and excimer laser irradiation crystallization (ELC). These methods could be concluded that the a-Si thin films are recrystallized into polycrystalline silicon thin film by applying additional energy. However, these technologies had some drawbacks as below: First, the SPC TFTs suffer a lot of intra-granular defects, which results in a bad performance and the long annealing time will limit the throughput to fabricate poly-Si thin film. Second, the metal induced crystallization (MIC) technology suffers from metal contamination incorporated into poly-Si thin film and the metal contamination will result in poor TFT performance. Third, although the excimer laser irradiation crystallization (ELC) technology is an useful technology to enlarge the grain size, there are still some disadvantages such as narrow laser process window for SLG and poor grain-size uniformity. In this thesis, therefore, we proposed a method, which is so called Diode-Pumped Solid-State (DPSS) Continuous Wave Laser-Crystallization (CLC). With the benefits of this longitudinal growth crystallization method, the poly-Si TFTs with high field-effect mobility have been fabricated.

At the first part, a new and simple CW laser crystallization is proposed to produce large longitudinally grown grains in the center region of the laser beam crystallized poly-Si via controlling the laser powers and the laser scanning speeds. However there are still small grains and polygonal grains in the edge and the transition region, which were SPC and PMG to SLG-like respectively, in spite of enlarging the laser powers or reducing the laser scanning speeds due to the Gaussian laser energy distribution. The small and polygonal grains in the channel region will deteriorate the performances of the TFTs. Therefore, multi-scan (overlapping method) scheme was proposed to achieve large area of longitudinal crystallization. According to the experimental results, the directionally longitudinal grains with tens of

micrometer, flat surface morphology, and excellent crystallinity were achieved without damages to the quartz substrates.

In the second part, the electrical characteristics of the continuous wave laser crystallized polycrystalline silicon thin-film transistors were also studied. In the SPC regime, the equivalent field-effect mobility, subthreshold swing, and threshold voltage were $19.4\text{cm}^2/\text{V}\cdot\text{s}$, $2.72\text{V}/\text{decade}$, and 7.93V , respectively. In PMG to SLG-like regime, the equivalent field-effect mobility, subthreshold swing, and threshold voltage were $86.9\text{cm}^2/\text{V}\cdot\text{s}$, $1.41\text{V}/\text{decade}$, and 0.296V , respectively. In longitudinal growth regime, high performance CLC poly-Si TFTs with equivalent field-effect mobility, subthreshold swing, and threshold voltage exceeding $281\text{cm}^2/\text{V}\cdot\text{s}$, $0.753\text{ V}/\text{decade}$, and -1.17V , respectively for n-channel devices have been fabricated without any hydrogenation treatment. It reflects that the larger grains with better crystallinity will possess the better electrical characteristics. Moreover such simple CW laser crystallization technique is promising for the applications in the future 3D- ICs.

誌謝

首先我要感謝我的指導教授 鄭晃忠博士，在碩士生涯中除了在實驗、研究與論文上細心的指導之外，老師做事態度上總是以認真、嚴謹、積極的正向態度面對，在待人處世方面更是謙恭溫和。老師的身教對我來說，不管是研究方向或是處理事情態度上，皆有深深地啟發與成長。

其次要感謝的是博班學長群們：在研究上總是為我指點迷津的逸哲，感謝他在碩士生涯中為我付出的精神及時間；當我做實驗做到快要崩潰，總是在一旁給我精神上支持的柏宇；不管在新廠或是在舊場常常會碰到的昭龍，做實驗時還好有你可以陪我解解悶；製程經驗豐富的俊諭，感謝在最後階段點出我的實驗瓶頸，以及最後階段不管是實驗或是論文上的幫忙；很有 sense 的昱智，每次與你討論問題，總有豁然開然的感覺；忙著準備資格考的宏顯，感謝材料分析機台方面的經驗傳授；奈米一哥加聰，常常到了晚餐時刻一起煩惱要吃什麼；奈米二哥萬霖，感謝您最後協助將元件做活了，以及一直在我耳邊覆誦安希教練曰：『現在放棄！比賽就結束了！』，真的很感謝您們。

另外，感謝傳授機台及實驗經驗的序恆學長，雖然畢業了還是很關心我。以及，在實驗或雜事上幫我超多的正國、旭航、雋荃、俊賢、佳信學弟們。以及同屆在無塵室內奮鬥的茜云、聖凱、邦祐、英彰、家名、俊凱、彥徵。當然，還有筠珊學姐，以及晏廷、宗哲、柏鈞、均宇、育荏學弟妹們一同在實驗室內製造歡樂的氣氛。當然，還有助理采綸，感謝她在行政上的幫忙，還有她那佛心來也的不定時點心，溫暖的實驗室夥伴每個人的胃。

還有一些已經畢業的學長姐們，包括國瑞、春乾、高照、大傳、君翰、育瑛、建穎、偉凱、仕煒、政欽，您們還沒畢業時對我的照顧。

感謝交大奈米中心及國家奈米實驗室所有幫助過我的工程師以及技術員們。

感謝從小到大的好友：聖淵、獲列、育維、育儒、士貴的一路相挺。

最後，我要將這篇論文獻給我的母親以及兩位哥哥們，因為您們的支持，我才能心無旁騖地完成碩士學業。

Contents

Abstract (in Chinese)	i
Abstract (in English)	iii
Acknowledgements (in Chinese)	vi
Contents	vii
Table Lists	x
Figure Captions	xi

Chapter 1 Introduction	1
1.1 Introduction of Low-Temperature Polycrystalline Silicon Thin-Film Transistors	1
1.2 Introduction of the Amorphous Silicon Thin Films Crystallization Technologies	2
1.2.1 Approaches to the Preparation of Poly-Si Thin Films by Utilizing Solid Phase Crystallization (SPC)	3
1.2.2 Approaches to the Preparation of Poly-Si Thin Films by Utilizing Metal Induced Crystallization (MIC)	4
1.2.3 Approaches to the Preparation of Poly-Si Thin Films by Utilizing Excimer Laser Irradiation Crystallization	5
1.3 Motivation	9

1.4 Thesis Organization10

Chapter 2 Basic Concepts of the Continuous Wave Laser Crystallization (CLC) and Fabrication Process of Polycrystalline Silicon Thin-Film Transistors Using Diode-Pumped Solid-State (DPSS) Continuous Wave Laser Crystallization (CLC)12

2.1 Introduction12

2.2 Fundamental Crystallization Mechanism of the Diode-Pumped Solid-State Continuous Wave Laser-Crystallized Poly-Si Thin Films14

2.3 Experiments15

2.3.1 The Setup of the Continuous Wave Laser Crystallization System15

2.3.2 Fabrication of the Polycrystalline Silicon Thin-Film Transistors Using Diode-Pumped Solid-State Continuous Wave16

2.3.3 Electrical Characterization17

Chapter 3 Investigation of the Laser Crystallized Polycrystalline Silicon Thin-Film Transistors19

3.1 Introduction19

3.2 Material Analyses of Polycrystalline Silicon Thin-Films Fabricated via Diode-Pumped Solid-State (DPSS) Continuous Wave Laser Crystallization (CLC)20

3.2.1 The Single-Scan Results of the Diode-Pumped Solid-State (DPSS) Continuous Wave Laser Crystallization (CLC)	20
3.2.2 The Multi-Scan Results of the Diode-Pumped Solid-State (DPSS) Continuous Wave Laser Crystallization (CLC)	25
3.2.3 Electrical Characteristics of Polycrystalline Silicon Thin-Film Transistors Using Diode-Pumped Solid-State (DPSS) Continuous Wave Laser Crystallization (CLC)	30
3.3 Summary	31
Chapter 4 Summary and Conclusions	33
References	65
Vita	75



Table Lists

Chapter 1

Table 1-1 Different excimer laser gases and their wavelengths λ35

Table 1-2 The comparisons of excimer laser and DPSS continuous wave laser.35

Chapter 3

Table 3-1 The characteristic of the laser beam. The laser power is 3.2W and the scanning speed is 40mm/s.36

Table 3-2 The FWHM and peak position of the Raman spectrum with various laser energies at the scanning speed of 50mm/s and the overlapping ratio of 90%.36

Table 3-3 The FWHM and peak position of the Raman spectrum with various scanning speeds at the laser power of 3.2W and the overlapping ratio of 90%.37

Table 3-4 The FWHM and peak position of the Raman spectrum with various overlapping ratio at the laser power of 3.2W and the scanning speed of 40mm/s.37

Table 3-5 The measured electrical characteristics of the n-channel TFT crystallized by DPSS CW laser. The scanning speed is 40mm/s, and the overlapping ratio is 90%.38

Table 3-6 The measured electrical characteristics of the n-channel TFT crystallized by DPSS CW laser. The scanning speed is 30mm/s, the laser power is 3.2W and the overlapping ratio is 90%.38

Figure Captions

Chapter 1

- Fig. 1-1 (a) The schematic illustration of the low energy regime corresponding to energy densities that partially melting the a-Si thin film.39
- Fig. 1-1 (b) The schematic illustration of the high energy regime corresponding to energy densities that completely melting the a-Si thin film.39
- Fig. 1-1 (c) The schematic illustration of the super lateral growth regime corresponding to energy densities that nearly completely melting the a-Si thin film.39

Chapter 2

- Fig. 2-1 The crystallization mechanism of continuous-wave laser longitudinal grain growth.40
- Fig. 2-2 The setup of DPSS continuous-wave laser crystallization.41
- Fig. 2-3 The key process procedures for fabricating CLC TFTs.43

Chapter 3

- Fig. 3-1 The energy profile of the continuous wave laser beam.44
- Fig. 3-2 The optical microscopy (OM) image of the laser beam crystallized poly-Si film, the laser power is 3.2W, the laser scanning speed is 40mm/s.44
- Fig. 3-3 The SEM image of the laser beam, the laser power is 3.2W, and the laser scanning speed is 40mm/s.45
- Fig. 3-4 The laser energies in the plane view and cross-section view of the laser beam.46

Fig. 3-5	The crystallization mechanism of the longitudinal growth in the center region.	46
Fig. 3-6	The crystallization mechanism of the PMG to SLG-like in the transition region.	47
Fig. 3-7	The Raman spectrum of the laser beam.	47
Fig. 3-8	The optical microscopy (OM) and scanning electron microscopy (SEM) images of crystallized poly-Si films with various laser energies at the scanning speed of 50mm/s and single-scan mode, and the laser powers were varied from 2.0W to 4.0W.	48
Fig. 3-9	The optical microscopy (OM) and scanning electron microscopy (SEM) images of crystallized poly-Si films with various laser speeds at the laser power of 3W and single-scan mode.	48
Fig. 3-10	The process window of crystallized poly-Si films at the center region, single-scan mode. Influence of laser power and laser scanning speed on the structure of grains. The SEM photographs of poly-Si film were crystallized at 2.0W, 2.8W, 3.5W, 4.5W, and the scanning speed is 50mm/s.	49
Fig. 3-11	The longitudinal-crystallized widths in the center region of the laser beam.	50
Fig. 3-12	The optical microscopy (OM) images of the longitudinal-crystallized width in the center region of the laser beam.	51
Fig. 3-13	The definition of the overlapping ratio of the laser beam.	52

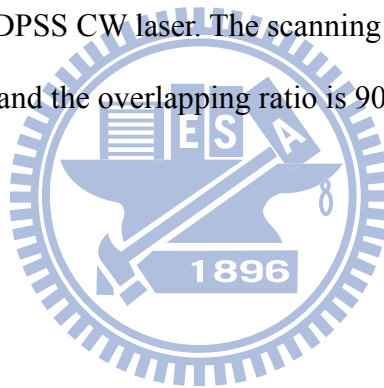
Fig. 3-14	The atomic force microscopy (AFM) images of the crystallized poly-Si films with various laser energies and scanning speeds at the overlapping ratio of 90%	53
Fig. 3-15	The 3-D images of the crystallized poly-Si films with various laser energies and scanning speeds at the overlapping ratio of 90%.	54
Fig. 3-16	The roughnesses of the crystallized poly-Si films with various laser energies and scanning speeds at the overlapping ratio of 90%.	54
Fig. 3-17	The Raman spectrum of crystallized poly-Si films with various laser energies at the scanning speed of 50mm/s and the overlapping ratio of 90%.	55
Fig. 3-18	The Raman spectrum of crystallized poly-Si films with various scanning speeds at the laser energy of 3.2W and the overlapping ratio of 90%.	56
Fig. 3-19	The XRD spectrum of crystallized poly-Si films with various scanning speeds at the laser power of 2W and the overlapping ratio of 90%.	57
Fig. 3-20	The XRD spectrum of crystallized poly-Si films with various laser powers at the scanning speed of 40mm/s and the overlapping ratio of 90%.	57
Fig. 3-21	The optical microscopy (OM) image of crystallized poly-Si films with various overlapping ratio from 10% to 30% at the scanning speed of 40mm/s and the laser power of 3.2W.	58
Fig. 3-22	The optical microscopy (OM) and scanning electron microscopy (SEM) of images crystallized poly-Si films with various overlapping ratio from 40% to 60% at the scanning speed of 40mm/s and the laser power of 3.2W.	60

Fig. 3-23 The optical microscopy (OM) and scanning electron microscopy (SEM) of images crystallized poly-Si films with various overlapping ratio from 70% to 90% at the scanning speed of 40mm/s and the laser power of 3.2W.62

Fig. 3-24 The Raman spectrum of crystallized poly-Si films with various overlapping ratios at the scanning speeds of 40mm/s and the laser power of 3.2W.62

Fig. 3-25 The transfer characteristics and output characteristics of the n-channel TFT crystallized by DPSS CW laser. The scanning speed is 40mm/s, and the overlapping ratio is 90%.63

Fig. 3-26 The transfer characteristics and output characteristics of the n-channel TFT crystallized by DPSS CW laser. The scanning speed is 30mm/s, the laser power is 3.2W, and the overlapping ratio is 90%.64



Chapter 1

Introduction

1.1 Introduction of Low-Temperature Polycrystalline Silicon Thin-Film Transistors

Thin-film transistors (TFTs) have become crucial devices of modern Active Matrix Liquid Crystal Displays (AMLCDs) and Active Matrix Organic Light Emitting Diodes (AMOLEDs) applications [1]-[5].

Generally, amorphous silicon (a-Si:H) TFTs are the pixel switching elements in AMLCD industry. Amorphous silicon TFTs exhibit low leakage current because of their high off-state resistivity. In addition, they are compatible with large glass substrate for low process temperature. However, the electrical characteristics of a-Si TFTs such as carrier mobility (typically below $1\text{cm}^2/\text{V}\cdot\text{s}$) are inadequate for peripheral circuits. That is, additional integrated circuits (ICs) are needed to support the function of gate drivers to drive a display panel. This will lead to high cost and poor reliability. On the other hand, low-temperature polycrystalline silicon (LTPS) TFTs process exhibit superior carrier mobility [6], greater device reliability, CMOS

process capability [7], and low temperature process compatibility. Therefore, LTPS TFTs have been investigated to achieve the goal of integrating peripheral circuit in a single panel, which is known as system on panel (SOP) [8]. Furthermore, LTPS TFTs have the potential to fulfill the three-dimensional integrated circuits. [9]

1.2 Introduction of the Amorphous Silicon Thin Films Crystallization Technologies

In polycrystalline silicon material, the grain boundaries will decrease the electrical characteristics of poly-Si TFTs because a lot of defects such as dangling bonds and strained bonds exist within them. These defects will result in higher threshold voltage (V_{th}), lower carrier mobility (μ), more gradual subthreshold swing (SS), larger leakage current, and poor long-term stability [10]. Therefore, how to reduce the defect densities in poly-Si films is an important subject for the fabrication of high performance poly-Si TFTs. There are two effective methods to reduce the defect state densities in poly-Si film, including the passivation of defect states both in the grains and grain boundaries [11]-[14], and the enlarging poly-Si grain size in the channel region [15]-[18]. Plasma hydrogenation is common used to passivate the defects in poly-Si film for attaining improvement of device performance and uniformity. Poly-Si TFTs after hydrogen passivation suffer from poor hot carrier endurance and a low thermal stability due to the weak Si-H bond. Reducing the defect states via enlarging poly-Si grain size is an intrinsic approach to single crystal Si material, which leads to the silicon-on-insulator like (SOI-like) device performance. There are several ways to enlarge the grain size, including solid phase crystallization

(SPC), metal induced crystallization (MIC), and laser irradiation crystallization. These methods could be concluded that the a-Si thin films are recrystallized into polycrystalline silicon thin film by additional energy.

1.2.1 Approaches to the Preparation of Poly-Si Thin Films by Utilizing Solid Phase Crystallization (SPC)

Solid phase crystallization method is an ordinary fabrication to transfer amorphous Si into poly-Si thin film via furnace annealing to supply thermal energy for 24 hours at temperature 600°C [19]. In order to match the low-temperature polycrystalline silicon (LTPS) thin film transistors (TFTs) fabrication with a maximum temperature below 600°C on glass substrate, the amorphous silicon thin film was deposited at 550°C using silane (SiH₄), and following the samples were placed in the furnace for 24 hours with the temperature of 600°C in nitrogen (N₂) ambient. [20]-[21].

The grain size of solid phase crystallized poly-Si thin film is several times larger than that of as-deposited poly-Si thin film. Besides, the surface morphology is much smoother in SPC poly-Si thin film than in as-doped ones. However, the SPC TFTs suffer a lot of intra-granular defects and result in a bad performance. The critical point is the fact that the annealing time is too long and this will limit the throughput to fabricate poly-Si thin film.

1.2.2 Approaches to the Preparation of Poly-Si Thin Films by Utilizing Metal Induced Crystallization (MIC)

The basic idea of metal induced crystallization (MIC) is furnace annealing, which is similar to solid phase crystallization (SPC). Several metals have been reported to be applied to MIC process, such as aluminum (Al), nickel (Ni), aurum (Au), and platinum (Pt). As a certain metal is deposited on a-Si, the a-Si films crystallized to poly-Si structure at a lower temperature than its SPC temperature, because the thermal budget of a-Si can be lowered by the introduction of metal impurities [22]-[25]. Compared to SPC, metal induced crystallization is able to reduce the annealing temperature ($<400^{\circ}\text{C}$) and process duration ($<5\text{hrs}$), therefore, higher throughput can be obtained.

Among these metals, Ni is the candidate for mainstream industrial application. Nickel silicide will be formed during process and the crystallization of silicon will start. Owing to the very small mismatch (0.4%) of crystal lattice constant between the $\langle 111 \rangle$ orientation faces of nickel silicide and crystalline silicon, the defects in crystal can be minimized [26]-[28].

Recently, it was found that metal induced lateral crystallization (MILC) rate could be enhanced remarkably and the crystallization temperature could be reduced to as below as 380°C due to the presence of an electrical field [29] - [33]. The phenomenon was explained by the enhanced diffusion of charged nickel through NiSi_2 precipitates in the applied electrical field [33].

Although the metal induced crystallization method can reduce the process temperature and raise the growth rate, metal contamination incorporated into poly-Si thin film is a noticeable problem which resulted in poor TFT performance, such as high leakage current, large kink current, worse subthreshold swing, and poor device stability. In order to suppress the metal contamination, using the metal solutions or depositing ultra-thin discrete metal layer on amorphous silicon are reported to fabricate poly-Si thin films [34]-[35].

1.2.3 Approaches to the Preparation of Poly-Si Thin Films by Utilizing Excimer Laser Irradiation Crystallization

Laser crystallization process in fabrication can produce large-grained poly-Si thin film with low intra-grain defects via liquid phase crystallization as compared with solid phase crystallization and metal induced crystallization. The laser irradiation crystallization process may be the most promising for grain growth with low intra-grain defects via liquid phase crystallization as compared with SPC and MIC, for silicon-on-insulator devices for microelectronics and thin-film transistors for displays has been receiving considerable attention [36]-[42]. The laser modes can mainly be divided into two types, pulse type and continuous wave laser type. Excimer lasers are the most effective and powerful UV light sources available today. In order to generate excimer laser radiation, a transient high voltage discharge is produced in a tube containing the laser gas. According to the laser gas used, laser radiation with

wavelengths between 157-351 nm can be obtained (as shown in table 1-1). The absorption coefficient of a-Si is quite high in the UV-light region of the excimer laser, it is possible to crystallize a-Si film without thermal damage to the glass substrates.[43] Besides, all excimer lasers are pulsed lasers. On the other hand, the continuous wave (CW) laser emits in green light by the diode-pumped solid-state (DPSS) laser source of Nd:YVO₄ (532nm) [44]. According to the reports of Akito Hara et al., long-wavelength laser energy of continuous-wave diode pumped solid-state laser (DPSSL) barely damaging glass substrates [45]. Thus, Both the excimer laser crystallization (ELC) and continuous-wave diode pumped solid-state laser (DPSSL) crystallization technologies were suitable for the fabrication of LTPS-TFTs.

The basic principle of excimer laser crystallization (ELC) is the phase transformation of silicon thin film from amorphous to single-crystal material via melting the silicon thin film within a very short time. Actually, the a-Si thin film is heated to the temperature of about 1200°C during laser irradiation. However, the high temperatures are only persistent for tens of nanoseconds during laser pulse duration.

The benefit of using ELC is the strong optical absorption of a-Si thin film to UV lights. During ELC process, a-Si thin films absorb the light, then rapidly melting and solidifying quickly, without significant heating the substrate and impurities contamination from the substrate diffusion into the silicon thin film. For the volume expansion from liquid to solid phase, surface roughness (usually called protrusion) occurs after the ELC process. It has been reported that increasing the laser shots will reduce the protrusion and obtain better crystallinity. The definition of laser shots is the overlaps between each laser shot, i.e., 20 shots correspond to 5% overlap per shot.

The poly-Si thin film fabricated by ELC suffers from narrow process window and instability of shot-to-shot laser energy, which lead to non-uniformity issue of grain structure. This technology yield high quality and large-grained poly-Si thin film for high-performance LTPS TFTs on glass or plastic substrate with high throughput.

According to the reports of James. S. Im et al., excimer laser crystallization of amorphous silicon thin films on foreign substrate can be divide into three transformation regimes with respect to the applied laser energy densities [46]-[47]. These are the partial-melting, full-melting, and near-complete-melting regimes, which are schematically illustrated in Fig. 1-1(a), Fig. 1-1(b), and Fig. 1-1(c), respectively.

Partial-melting regime (Low energy density regime)

In the partial melting regime, the incident laser energy density is larger than the threshold energy of melting of a-Si films. The applied laser energy density can cause only surface melting of a-Si thin films but not the entire silicon films (i.e., melting depth < film thickness). Therefore, a-Si thin film can be partially melted and subsequently be recrystallized from the underlying continuous layer of remained solid Si. In this regime, the poly-Si grain size increases with the increases of the laser energy density. In addition, it is characterized that explosive crystallization of a-Si thin film occurs at the onset of the transformation and follows by vertical grain growth, and competitive occlusion of grains [48]. The early trigger of explosive crystallization may be attributed to the presence of microcrystalline clusters or to the presence of impurities in the silicon films.

Complete –melting regime (High energy density regime)

In the complete melting regime, the incident laser energy density is sufficient

high to cause the complete melting of the entire a-Si thin films. Since the glass substrate is amorphous structure, epitaxial layer growth from the substrate is not possible. For the complete-melting Si thin film, a deep supercooling of the liquid silicon film leads to homogeneous nucleation before the transformation of poly-Si in solid phase [49]-[50]. In this regime, the final microstructure is insensitive to the applied laser energy densities. Fine-grained and small-grained poly-Si thin films are attained due to the low substrate temperature. In addition, a phenomenon of amorphization is observed in thinner silicon films [51].

Near-complete-melting regime (Super-lateral-growth regime)

In the near-complete-melting regime, the incident laser energy density leads to a complete melting a-Si thin film consisting of un-melted discrete silicon islands (i.e. melting depth \approx film thickness). James. S. Im et al. indentified the third transformation regime, the end of the low energy density regime and the beginning of the high energy density regime, in a narrow experimental window [52]-[53]. In this regime, large-grained poly-Si films with grain sizes many times larger than the film thickness are observed. Since the grain size is much larger than that in the other two transformation regimes, Im named it super lateral growth (SLG) regime due to its unique nature [53]. Based on Im' model, it is argued that the un-melted portion of the underlying Si no longer forms a continuous layer but instead consist of discrete solid silicon islands which are separated by small local regions in the completely melting silicon film. The un-melted silicon islands act as nucleation seeds and lateral grain growth can proceed toward the complete melting region. Therefore, a significant lateral growth takes place before the impingement of the grain grown from the other

side depending on the separation distance between these seeds. There is a limit for the maximum lateral growth distance; however, since the continuous cooling of the liquid layer via thermal conduction to the underlying substrate eventually would lead to copies nucleation of solids in bulk liquid ahead of the interface. According to the SLG model, the super lateral grain growth distance will increase with thicker film thickness, higher substrate temperature, lower thermal conductivity of the substrate, and longer laser pulse duration. In addition, the applied energy density for super lateral growth regime increases with thicker film thickness, shorter laser pulse duration, higher thermal conductivity of the substrate, and lower substrate temperature. It is concluded that the lateral grain growth is resulted from the thermal gradient between the solid and liquid interface and the lateral grain growth distance is determined by the quenching rate of liquid silicon and the residual solid Si seed distance. As a result, the SLG distance can be prolonged by enlarging the lateral thermal gradient and increasing the solidification duration.

However, a very non-uniform grain size distribution is observed in the SLG regime due to the fluctuation of pulse-to-pulse laser energy density, non-uniform laser beam profile, and non-uniformity of a-Si thin film thickness. The non-uniform grain distribution cause device degradation and poor device-to-device uniformity as the laser energy density is controlled in the SLG regime. It is very undesirable for device and circuits applications.

1.3 Motivation

The low temperature polycrystalline silicon (LTPS) thin film transistors (FTFs)

have been widely applied to high-definition active matrix liquid crystal displays (AMLCDs) and active matrix organic light emitting displays (AMOLEDs). The quality of the polycrystalline silicon thin film taking as the active layer of the device plays an obviously strong character in the device performance. In order to achieve a high performance LTPS TFTs, we introduced the CW laser longitudinal crystallization method to reduce the defects of polycrystalline silicon thin film. The defects in the inter-grain will decrease the electrical characteristics of the device, including the decreasing the carrier mobility and increasing the leakage current of the device. In addition, CW laser lateral crystallization has the advantage of simple process, superior power stability, wide laser process window for large grains, and easy maintenance. The comparisons of excimer laser and DPSS continuous wave laser are listed in Table 1-2. Among the pulse type laser crystalline methods, the Sequential Lateral Solidification (SLS) crystallization method proposed by Robert S et al. has been achieve high device performance (carrier mobility = 200~300 cm²/V-s), however, the grain size is limited to 3μm [54]. In order to produce ultra-large silicon grains in large area substrates for SOP, 3D-ICs, and solar cell applications, we proposed a simple method to achieve the high quality polycrystalline silicon film, which is so called diode pumped solid state (DPSS) continuous wave laser crystallization (CLC) method. The grain size can be achieved to several tens micro-meter to fabricate the high performance polycrystalline silicon thin-film transistors.

1.4 Thesis Organization

In chapter 1, an overview of LTPS technologies was given. The polycrystalline

silicon crystallization processes were brief explained. The motivations of this thesis were explored to introduce the thesis.

In chapter 2, the setup of continuous wave laser annealing system was brief introduced and the fabrication processes of polycrystalline silicon thin-film transistors using diode-pumped solid-state (DPSS) continuous wave laser crystallization (CLC) were described in detail.

In chapter 3, the CW laser-crystallized poly-Si thin film was analyzed by several material analyses, including SEM, Raman, AFM, XRD, and the factors that affected the final crystallization microstructure were also investigated, including the laser power, the laser scanning speed of the single-scan mode, and the overlapping ratio of the multi-scan mode. By analyzing the microstructure of poly-Si films, CW laser crystallization mechanism of a-Si films were presented and the electrical characteristics of CLC poly-Si TFTs were discussed.

Finally, summary and conclusions were given in chapter 4.

Chapter 2

Basic Concepts of the Continuous Wave Laser Crystallization (CLC) and Fabrication Process of Polycrystalline Silicon Thin-Film Transistors Using Diode-Pumped Solid-State (DPSS) Continuous Wave Laser Crystallization (CLC)



2.1 Introduction

Recently, low-temperature polycrystalline silicon (LTPS) technology has been the most promising method to fabricate high performance thin film transistors (TFTs). As compared to conventional a-Si TFTs, LTPS TFTs using excimer laser crystallization (ELC) technology have been promise to integrate display driver circuits on glass substrate such as integrated ambient light sensing, memory in pixel,

integrated touch, ultra-low power display driving, advanced active matrix liquid crystal displays (AMLCDs) driving, and advanced active organic light emitting displays (AMOLEDs) driving.

The demands for thin, light-weight, compact, and high resolution displays are getting stronger in the mobile applications. Integrating large scale circuits in small area and reducing power consumption both are requisite features for mobile applications with high resolution or more functional LCDs [55] In addition, as the mobility of poly-Si TFT is approaching that of single crystalline silicon, it is possible to realize system-on-panel (SOP) application which build an integrated drive circuit, sensors, controller IC, CPU as well as display on glass[56]. However, the present conventional ELC LTPS technology can not meet the requirements owing to the large variation in electrical characteristics caused by grain boundaries in the channel regions. Although high-performance ELC LTPS TFTs can be fabricated by optimizing the applied laser energy density and increasing the shot density per area, ELC LTPS TFTs suffer from poor uniformity of device performance due to the narrow laser process window for producing large-grain poly-Si. The fluctuation of pulse-to-pulse laser energy density, non-uniform laser beam profile, and non-uniformity of a-Si thin film thickness make laser energy density hard to hit the super lateral growth (SLG) regime everywhere [57]-[58]. Non-uniform and randomly distributed poly-Si grains will result in large variation of TFT performance when the laser energy density is controlled in the SLG regime, especially for small geometry TFTs [59]-[61]. Increasing laser shot density per area may improve the crystallization uniformity and promote the secondary grain growth [62], however, the mass production throughput will decrease. Besides, excimer laser annealing has some essential drawbacks such as complex optical system, high facility cost, troublesome maintenance, and poor output

energy stability. As a result, novel crystallization methods are strongly demanded to enhance both the device performance and uniformity for next generation LTPS TFTs, thus we proposed so-called diode pumped solid state (DPSS) continuous wave laser crystallization (CLC) method. The grain size can be achieved to several tens micrometers to fabricate the high performance polycrystalline silicon thin-film transistors.

2.2 Fundamental Crystallization Mechanism of the Diode-Pumped Solid-State Continuous Wave Laser-Crystallized Poly-Si Thin Films

Fig. 2-1 shows the crystallization mechanism of continuous-wave laser longitudinal grain growth, the directional-controlled poly-Si via controlling the laser power and the laser scan speed. A lateral temperature gradient can be created between the adjacent areas and there must be un-melting solid Si to act as the seeds for lateral crystallization. By completely melting the a-Si thin film in a certain region using CW laser and solidified poly-Si films at the adjacent area, a large lateral temperature gradient will exist between the complete melting high-temperature liquid-phase region and un-melting low-temperature solid-phase seeds, and grains will grow laterally towards the complete melting region from the un-melting solid seeds. As a result, if the temperature gradient is stable in the liquid-solid interface by suitable laser power and laser scan speed, directional lateral grain growth of several tens micrometers can be achieved easily. The lateral grain growth will eventually be arrested by lateral grains grown from the other side.

2.3 Experiments

2.3.1 The Setup of the Continuous Wave Laser Crystallization System

The principle setup of diode-pump solid-state (DPSS) continuous-wave laser crystallization equipment is shown in Fig. 2-2. The laser light source of this system is the frequency-doubled diode-pumped solid-state Nd:YVO₄ continuous-wave laser, operating at the wavelength of 532nm. The laser can achieve a maximum peak output power 18W. The sample is crystallized and scanned via laser beam scanning and overlapping on the x-y translation stage. The overlap helps to improve the uniformity of CW laser-crystallized poly-Si thin films because the crystallinity of poly-Si film in the middle regions of the laser beam is better than that in the edges of laser beam. Crystallization of large area is achieved by moving the sample under the laser beam via controlling the movement of the x-y translation stage. The scanning direction paralleled the short axis of the laser beam. The laser power and the velocity of the x-y translation stage be adjusted by the computer individually during crystallization process. In addition, the crystallization experiments can be performed at either room temperature or 500°C. The maximum laser beam size is about 370um * 300um.

2.3.2 Fabrication of the Polycrystalline Silicon Thin-Film Transistors Using Diode-Pumped Solid-State Continuous Wave

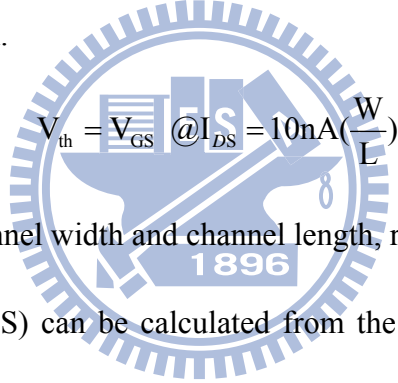
Fig. 2-3 shows the key processes for the fabrication of poly-Si TFTs crystallized by using frequency-doubled diode-pumped solid-state Nd:YVO₄ continuous-wave laser irradiation. At first, a 2000 Å-thick a-Si layer was deposited by pyrolysis of pure silane (SiH₄) with low pressure chemical vapor deposition (LPCVD) at 550°C on quartz wafer. Then, after standard RCA clean process, the samples were then subjected to green laser crystallization by diode-pumped solid-state continuous-wave laser ($\lambda=532\text{nm}$). During the laser irradiation, the samples were located on a substrate at room temperature. The power of laser energy density, the laser scan speed, and the laser overlap ratio were varied. After defining the device active region and standard RCA clean process, a 1000 Å-thick tetraethyl orthosilicate (TEOS) gate oxide layer was deposited by LPCVD at 700°C. Then, a 2000 Å-thick a-Si thin film was deposited by LPCVD at 550°C for gate electrode. The a-Si thin film and gate oxide were etched by reactive ion etching (RIE) to form the gate electrode. A self-aligned phosphorous ion implantation with dose of $5 \times 10^{15} \text{ cm}^{-2}$ was carried out to form gate, source and drain regions. Next, a 5000 Å-thick TEOS passivation oxide was deposited by LPCVD at 700°C and the dopants were activated by this step. After contact hole opening by wet etching, aluminum thin film with a thickness of 6500 Å was deposited by electron beam evaporator system at 8×10^{-7} torr, and the Al metal pad were patterned by wet etching to complete the fabrication of CW laser annealing poly-Si TFTs.

Several material analysis techniques were used to investigate. They include

optical microscopy (OM), scanning electron microscopy (SEM) analysis, atomic force microscopy (AFM), Raman spectroscopy analysis, X-ray diffraction (XRD) analysis.

2.3.3 Electrical Characterization

Current-voltage (I-V) characteristics of the fabricated devices were measured using a semiconductor parameter analyzer of Agilent technologies 4156C. The threshold voltage was defined as the gate voltage required to achieve a normalized drain current of $I_{DS} = (W/L) * 10^{-8}$ A at $V_{DS} = 0.1V$, i.e., V_{th} is extracted approximately at $I_D = 10nA$.



$$V_{th} = V_{GS} @ I_{DS} = 10nA \left(\frac{W}{L} \right)$$

where W and L are the channel width and channel length, respectively.

The subthreshold swing (SS) can be calculated from the subthreshold current in the weak inversion region by

$$SS = \min \left(\frac{\partial \log(I_{DS})}{\partial V_{GS}} \right)^{-1} @ V_{DS} = 0.1V$$

and the field-effect mobility (μ_{FE}) is determined by

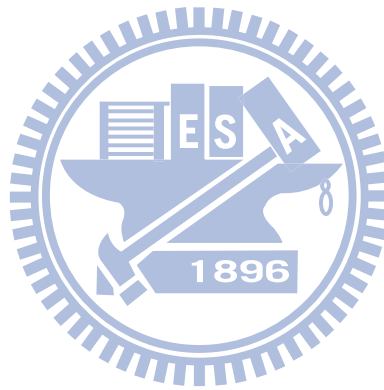
$$\mu = \frac{g_m}{C_{ox} \left(\frac{W}{L} \right) V_{DS}} (@ V_{DS} = 0.1V)$$

where g_m is the maximum transconductance and C_{ox} is the gate capacitance per unit area. The transconductance (g_m) is extracted by the differentiation of I_{DS} to V_{GS} .

$$g_m = \frac{\partial I_{DS}}{\partial V_{GS}} (@ V_{DS} = 0.1V) \cong \left(\frac{W}{L} \right) \mu C_{ox} V_{DS}$$

$$I_{\text{on}}/I_{\text{off}} = I_{\text{max}}/I_{\text{min}}@V_{\text{DS}} = 3V$$

Finally, the $I_{\text{on}}/I_{\text{off}}$ current ratio was defined at $V_{\text{DS}} = 3V$.



Chapter 3

Investigation of the Laser Crystallized Polycrystalline Silicon Thin-Film Transistors



3.1 Introduction

Large-grained poly-Si thin films always result in high-performance LTPS TFTs owing to the fewer defect traps in the grain boundaries and interior grains. Hence, recently, solid-state laser crystallizations of amorphous silicon, including pulsed YAG 2ω green laser [63], selectively enlarging laser crystallization (SELAX) [64], double-pulsed laser annealing [65], and the diode-pumped solid-state (DPSS) continuous wave laser lateral crystallization (CLC) [66], have been widely studied by effectively enlarging the poly silicon grain size for high-performance TFTs as compared with conventional excimer laser crystallization. Among these crystallization technologies, diode-pumped solid-state continuous wave laser lateral crystallization proposed by Hara et al. has been demonstrated to fabricate high-performance poly-Si

TFTs on non-alkali glass substrate because of the large directional silicon grains [66]. In addition, CW lateral crystallization has the advantages of simple process, superior power stability, wide laser process window for large grains, high throughput, and easy maintenance. Besides, it is difficult to achieve higher mobility using the conventional ELC crystallization method due to small grains. In order to produce ultra-large silicon grains in large area substrates for SOP, 3D-ICs, and solar cell applications, the high performance polycrystalline silicon thin-film transistors using diode-pumped solid-state continuous wave laser annealing in this chapter will be discussed.

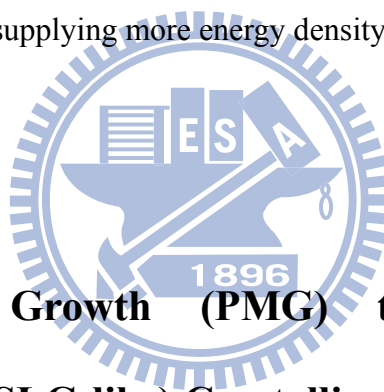
3.2 Material Analyses of Polycrystalline Silicon Thin-Films Fabricated via Diode-Pumped Solid-State (DPSS) Continuous Wave Laser Crystallization (CLC)

3.2.1 The Single-Scan Results of the Diode-Pumped Solid-State (DPSS) Continuous Wave Laser Crystallization (CLC)

In order to obtain the longitudinal grains, the laser power and laser scanning speed were varied and the process window of producing longitudinal grain can be obtained (This was discussed in the follow section).

Fig. 3-1 shows the energy profile of the continuous wave laser beam. Because the emitting light of CW laser is Gaussian distribution, its intensity lateral is non-uniform laterally, and the central intensity is the highest and outflow boundary is

lowest. The CW laser power of 3.2W and the laser scanning speed of 40mm/s were supplied to crystallize the a-Si film. Fig. 3-2 shows the optical microscopy (OM) image of the laser beam crystallized poly-Si film, and its corresponding SEM images are shown in Fig. 3-3. From the OM image, we classify the poly-Si thin film into four regions after the laser annealing. They are the a-Si region, the edge region, the transition region, and the center region of the laser beam from the outer region to the inner region. From the Fig. 3-3, the grain sizes were increasing from the edge region to the center region, and the grain shapes were changed from the small circle grain to the polygon and longitudinal grains. This is because the laser energy is increasing from the edge region to the center region and this will be useful for crystallization owing to the higher power supplying more energy density.



Partial Melting Growth (PMG) to Super Lateral Solidification-like (SLG-like) Crystallization

Fig. 3-4 shows the corresponding laser energies in the plane view and cross-section view of the laser beam. The liquid-solid interface was located on the transition region. In this region, the grain growth was partial melting growth (PMG) to super lateral solidification-like (SLG-like) crystallization owing to a vertical temperature gradient in the liquid phase, as shown in the Fig. 3-6. The heat flow is from the higher temperature (the top part of the silicon film) to the lower temperature (the bottom part of the silicon film). The un-melted grains in the top part of the silicon film act as the seeds, thus the grains grow from the bottom of the silicon film to the top part of that, and this is so-called partial melting growth (PMG) to super lateral

solidification-like (SLG-like) crystallization.

Longitudinal Growth Crystallization

Fig. 3-5 shows the crystallization mechanism of the longitudinal growth in the center region. A scanning direction temperature gradient was from the present melting region to the solidified region. The crystallization direction was the same with the scanning direction due to the strong scanning-direction temperature gradient in the liquid-solid interface and continuous energy was supplied. Thus, the post annealing regions act as the seeds and start to crystallize the a-Si thin film from this region to the present melting region. Because the crystallization direction is parallel with the scanning direction, a longitudinal grain can be obtained, and we can reduce the probability of the electron scattering to improve the device performance by using this region as the channel region of the TFTs.

The characteristics of the laser beam were summarized in the Table 3-1, and the crystallinity dependence on the location of the beam profile was shown in the Fig. 3-7. As a result, the crystallinity of the center region is better than other regions due to the maximum power obtained from the continuous power supplying.

Laser Energy Effect

Fig. 3-8 shows the optical microscopy (OM) and scanning electron microscopy (SEM) images of crystallized poly-Si films with various laser energies at the scanning

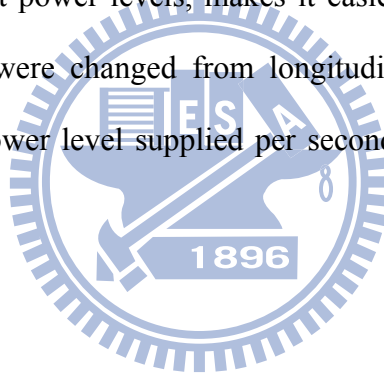
speed of 50mm/s and single-scan mode. And the laser powers were varied from 2.0W to 4.0W. The grain sizes were increasing with increasing the laser power due to the higher power supplying more energy density and reducing the cooling rate at the same time. The process window was shown in Fig. 3-10, and the longitudinal large grains were achieved about in 0.8W. Thus, the process by using diode-pumped solid-state continuous wave laser crystallization resulted in the better uniformity of the electrical characteristics of TFTs and it was easily to fabricate the high performance poly-Si TFTs.

Laser Scanning Speed Effect

Fig. 3-9 shows the optical microscopy (OM) and scanning electron microscopy (SEM) images of crystallized poly-Si films with various laser speeds at the laser power of 3W and single-scan mode. The grain sizes were increasing with decreasing the scanning speed because the slower scanning speeds result in longer melting duration. The melting duration affects primarily the quality of the silicon films, the slower scanning speeds result in longer melting duration and the grain sizes become larger. The longitudinal large grain were achieved in different scanning speeds, and this implied that the power stability of the diode pumped solid state continuous wave laser is better than that of the excimer laser. Thus, it resulted in the better uniformity of the electrical characteristics and was easily to fabricate the high performance poly-Si TFTs by using diode-pumped solid-state continuous wave laser crystallization.

Process Window

From the results of the laser energy effect and the laser scanning speed effect, the dependency of the structure of the poly-Si film on the laser power and the laser scanning speed for a 200nm thick Si film can be summarized in Fig. 3-10. After the CW laser annealing, the poly-Si thin films can be classified into four crystallization conditions, which are small grain region (SPC regime), polygonal grain region (partial liquid phase crystallization), longitudinal grain (fully liquid phase crystallization) and ablation region (The laser energy is too large.). The CLC method, with wide range of scanning speeds and output power levels, makes it easier to form large longitudinal grains. The grain shapes were changed from longitudinal to polygonal and small circle by decreasing the power level supplied per second or increasing the scanning speed [67].



Longitudinal-Crystallized Widths in the Center Region

Fig. 3-11 shows the longitudinal-crystallized widths in the center region of the laser beam, and the corresponding optical microscopy (OM) images were shown in the Fig. 3-12. Increasing the laser power or decreasing the scanning speed resulting in a longer solidification time were useful to enlarge the width of the center region with longitudinal grains for the channel region of the TFTs.

3.2.2 The Multi-Scan Results of the Diode-Pumped Solid-State (DPSS) Continuous Wave Laser Crystallization (CLC)

We have already successfully converted the a-Si films in the center region into the poly-Si films with ultra large and high-quality grains by using the long axis scanning. However, the edge and transition regions of that were still small and polygon grains which resulting in non-uniform quality of the CLC poly-Si film. And the defects in the edge and transition regions in the channel deteriorate the performance of the CLC poly-Si TFTs. Thus, the multi-scan technology for improving the uniformity of the poly-Si films was also investigated.



Overlapping Ratio

Fig. 3-13 shows the definition of the overlapping ratio of the laser beam and the equation is shown bellow. The pitch is the distance between the present scan and previous scan, and the maximum beam width (370 μ m) is defined as the width of the laser beam in the maximum laser power of 18W and the scanning speed of 5mm/s via long axis scanning.

$$\text{Overlapping Ratio} = \left(1 - \frac{\text{Pitch}}{\text{Maximum BeamWidth}}\right) * 100\%$$

The Overlapping Ratio of 90% with Various Laser Powers and Scanning Speeds

In order to improve the uniformity of the laser crystallized poly-Si film, the overlapping ratio of 90% was studied because such high overlapping ratio will make the crystallinity of the laser crystallized poly-Si film consistent. Fig. 3-14 shows the AFM images of the crystallized poly-Si films with various laser energies and scanning speeds at the overlapping ratio of 90%. In the as-deposited regime, the silicon remained a-Si, and thus the roughness is fairly smooth. In the solid phase crystallization (SPC) regime with the laser power of 2W the roughness is still fairly smooth and about 2nm. In the PMG to SLG-like regime, the grain growth started from the bottom part of the silicon film to the top part of the silicon film. In the process of the grain growth, the grains impinged on each other, which resulted in rough mountain ridge-like morphology, and the roughness of this regime is about from 19nm to 27nm. In the longitudinal growth regime, the roughness is about 13nm to 18nm because the grain boundary does not form a ridge at the junction of grain boundaries and its surface morphology is flatter than the PMG to SLG-like regime [67]-[68]. The longitudinal grains can be clearly distinguished and the grains extend in tens of micro-meter. The reason is that the 10% density change between solid and liquid phases of silicon provides a driving force for the mass transport induced by surface tension in the molten silicon during the laser crystallization. Fig. 3-15 shows their 3-D images of the crystallized poly-Si films with various laser energies and scanning speeds at the overlapping ratio of 90%, and their roughness were compared in the Fig. 3-16.

Fig. 3-17 shows the Raman spectrum of crystallized poly-Si films with various

laser energies at the scanning speed of 50mm/s and the overlapping ratio of 90%. The FWHM and peak position of the Raman spectrum were summarized in the Table 3-2. From the experimental results, the higher laser energy seems to be beneficial for improving the grain quality due to larger energy density.

Fig. 3-18 shows the Raman spectrum of crystallized poly-Si films with various scanning speeds at the laser power of 3.2W and the overlapping ratio of 90%. The FWHM and peak position of the Raman spectrum were summarized in the Table 3-3. From the experimental results, the slower scanning speed seems to be beneficial for improving the grain quality due to longer melting duration. The smaller FWHM of the peak of the Raman shift exhibits the better crystallinity of the silicon film.



Fig. 3-19 shows the XRD spectrum of crystallized poly-Si films with various scanning speeds at the laser power of 2W and the overlapping ratio of 90%. Fig. 3-20 shows the XRD spectrum of crystallized poly-Si films with various laser energies at the scanning speed of 40mm/s and the overlapping ratio of 90%. From the experimental results, it is well known that the (111) texture has the minimum free energy of the Si surface. In order to minimize the surface free energy, the longitudinal grain growth will tend to result in a restricted orientation of (111). On the other hand, as the scanning speed decreasing or the power energy increasing, the interface between melting and cooling regions of Si thin films has a tendency to take the (400) surface [69], which is beneficial for improving the performance of the TFTs.

The Overlapping Effect

In order to improve the quality of the a-Si thin film, different overlapping

conditions were investigated. According to the crystallinity of the overlapping regions, we can classify the overlapping states into three conditions:

First, the optical microscopy (OM) images of crystallized poly-Si films with various overlapping ratio from 10% to 30% at the scanning speed of 40mm/s and the laser power of 3.2W were shown in the Fig. 3-21. In this regime, the non-reaction region overlapped each other, and amorphous film remained in the overlapping regions.

Second, the optical microscopy (OM) and scanning electron microscopy (SEM) images of crystallized poly-Si films with various overlapping ratio from 40% to 60% at the scanning speed of 40mm/s and the laser power of 3.2W were shown in the Fig. 3-22. In this regime, the small grain or polygonal grain remained in the overlapping regions: In the overlapping ratio of 40% regime, because the edge regions were overlapped each other, the small grain and polygonal grain remained in the overlapping regions. In the overlapping ratio of 50% regime, because the edge and transition regions were overlapped each other, the polygonal grain remained in the overlapping regions. In overlapping ratio of 60% regime, because the transition regions were touched each other, the polygonal grain remained in the overlapping regions.

Third, the optical microscopy (OM) and scanning electron microscopy (SEM) images of crystallized poly-Si films with various overlapping ratio from 70% to 90% at the scanning speed of 40mm/s and the laser power of 3.2W were shown in the Fig. 3-23. In this regime, the center region were overlapped each other, and only longitudinal grains were found in the overlapping regions.

Shuntaro Fujii and Yuta Sugawara et al. reported that the absorption coefficient

of poly-Si for the green laser is much smaller than that of a-Si [70]-[72]. The a-Si films effectively absorbed CW laser beams, but the recrystallized Si thin film scarcely absorbed CW laser beams. It was considered that a-Si and microcrystals, which were not recrystallized by previous CW laser annealing. The a-Si and microcrystals were melted during the overlapping of CW laser irradiation and started to recrystallize from the peripheral crystal grains recrystallized by previous CW laser annealing [69]. In other words, in the overlapping ratios of 40%~60%, the absorption coefficient of polygonal and longitudinal poly-Si grains was small, the laser power was almost not be used to recrystallize the previous polygonal and longitudinal grains. In the overlapping ratio of 70%~90%, no matter how the crystallinity of the silicon thin film crystallized by the previous laser annealing was, the high energy in the laser beam center region of the following laser annealing will melt them and form longitudinal grains. However, the edge and transition regions of the following laser annealing will not destroy the previous polygonal and longitudinal grains. Thus, the large area of longitudinal crystallization can be achieved by using the overlapping scanning technology.

Fig. 3-24 exhibits the Raman spectrum of crystallized poly-Si films with various overlapping ratios at the scanning speeds of 40mm/s and the laser power of 3.2W. The FWHM of the Raman spectrum were shown in the Table 3-4, and the crystallinity were better with increasing the overlapping ratio.

3.2.3 Electrical Characteristics of Polycrystalline Silicon

Thin-Film Transistors Using Diode-Pumped Solid-State (DPSS) Continuous Wave Laser Crystallization (CLC)

Akito Hara et al. reported that the grain boundary acts as a strong scattering center for carrier transportation. Thus, the average field-effect mobility of parallel TFTs is larger than that of perpendicular TFTs [67]. Fig. 3-25 shows the transfer characteristics and output characteristics of the n-channel TFT crystallized by DPSS CW laser. The scanning speed was 40mm/s, the overlapping ratio was 90%, and the channel is parallel with the scanning direction. The measured electrical characteristics were summarized in the Table 3-5. From the experimental results, in the SPC regime (with the laser power of 2W), the equivalent field-effect mobility, subthreshold swing, and threshold voltage were $19.4\text{cm}^2/\text{V}\cdot\text{s}$, $2.72\text{V}/\text{decade}$, and 7.93V , respectively. In PMG to SLG-like regime (with the laser power of 2.4W), the equivalent field-effect mobility, subthreshold swing, and threshold voltage were $86.9\text{cm}^2/\text{V}\cdot\text{s}$, $1.41\text{V}/\text{decade}$, and 0.296V , respectively. In longitudinal growth regime (with the laser power of 3.2W), high performance CLC poly-Si TFTs with equivalent field-effect mobility, subthreshold swing, and threshold voltage were $281\text{cm}^2/\text{V}\cdot\text{s}$, $0.753\text{V}/\text{decade}$, and -1.17V , respectively. These n-channel devices have been fabricated without any hydrogenation treatment. The CLC TFTs fabricated in longitudinal growth regime with large directional grains demonstrated the higher driving current and field-effect mobility, which were attributed to high quality poly-Si thin films with fewer grain boundaries in the device channel region. The CW laser-crystallized TFTs whose

channel is parallel with the scanning direction have been demonstrated on the quartz wafer with champion field-effect mobility of $388\text{cm}^2/\text{V}\cdot\text{s}$ for n-channel devices as shown in the Fig. 3-26 and Table 3-6.

3.3 Summary

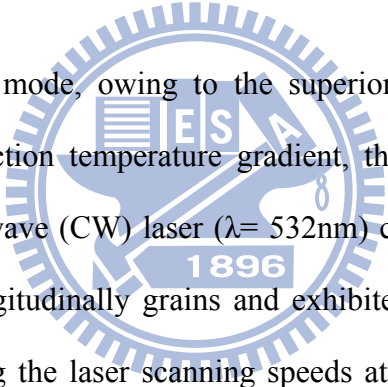
A simple diode-pumped solid-state (DPSS) continuous-wave (CW) laser is proposed to produce longitudinal grain growth via controlling the laser scanning speeds and the laser powers. The CW laser-crystallized poly-Si thin films were analyzed by several material analyses, including SEM, Raman, AFM, XRD, and factors that affected the final longitudinal crystallization microstructure were also investigated, including the laser scanning speed, the laser power, and the overlapping ratio. From the SEM images, the four kinds of silicon grain structure in the CW laser crystallized poly-Si thin films with single-scan mode were obviously distinguished. The a-Si films in the center region have been successfully converted into the poly-Si films with ultra large and high-quality grains by using the long axis scanning. However, the edge and transition regions of that were still small grains which resulting in the non-uniform quality of the CLC poly-Si film. And the defects in the edge and transition regions in the channel degraded the performance of the CLC poly-Si TFTs. Thus, the multi-scan technology for improving the uniformity of the poly-Si films was studied. In order to crystallize large area with directional large grains for high TFT performance with good uniformity, the CW laser with an overlapping 90% was performed. From the SEM and AFM analyses, the directional large grains were easy formed by CW laser longitudinal crystallization directional

large grains (5 μ m*100 μ m) owing to the continuous energy supply and slow cooling rate of the molten Si without damage to the quartz substrates. In addition, the CW laser-crystallized TFTs have been demonstrated on the quartz wafer with champion field-effect mobility of 388cm²/V-s for n-channel devices.



Chapter 4

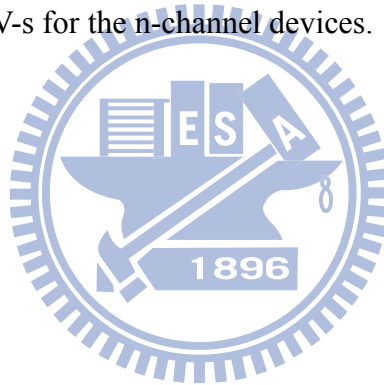
Summary and Conclusions



In single-scan mode, owing to the superior power stability (1%) and strong scanning-direction temperature gradient, the diode-pumped solid-state (DPSS) continuous-wave (CW) laser ($\lambda=532\text{nm}$) crystallization was proposed to produce large longitudinally grains and exhibited wide process window of 0.8 W via controlling the laser scanning speeds at 50 mm/s and laser powers from 3.0 W to 3.8 W. The grain sizes of the poly-Si film were about $50\text{ nm} \times 50\text{ nm}$, $1\text{ }\mu\text{m} \times 1\text{ }\mu\text{m}$, and $5\text{ }\mu\text{m} \times 100\text{ }\mu\text{m}$ corresponding to the SPC, PMG to SLG-like, and longitudinal growth regimes. Moreover, with increasing the laser power and decreasing the scanning speed correspond to a larger energy density and longer solidification time, respectively; it was useful to enlarge the width of the center region with longitudinal growth.

However, the edge and transition regions corresponding to SPC and PMG to SLG-like regimes can be suppressed using multi-scan mode and the grain size was consequently achieved about 100 μm over the crystallized area with

the minimum overlapping ratio of 70%. According to the Raman analysis, the FWHMs of Raman shift of the CLC poly-Si film were decreased from 6.25 cm^{-1} to 5.11 cm^{-1} with increasing the laser power from 2W to 3.2W and, besides, the field effect mobility of the thin film transistors was increased from 19.4 to 281 $\text{cm}^2/\text{V-s}$ due to the better crystallinity and larger grain size. The roughnesses of the longitudinal grains were between 13.308 nm and 18.67 nm, and the roughnesses of the PMG to SLG-like grains were between 19.00 nm and 27.03 nm. Therefore, the CLC longitudinal grain structure is more suitable for the high-performance SOP devices. Consequently, the CW laser-crystallized TFTs have been demonstrated on the quartz wafer with champion field-effect mobility of 388 $\text{cm}^2/\text{V-s}$ for the n-channel devices.



Tables

Laser gas	XeF	XeCl	KrF	KrCl	ArF	F ₂
Output wavelength λ (nm)	351	308	248	222	193	157

Table 1-1 Different excimer laser gases and their wavelengths λ .

Table 1-2 The comparisons of excimer laser and DPSS continuous wave laser.

Laser type	Pulse laser	CW laser(DPSS)
Irradiation time	Few tens ns	Several μ s
wavelength	UV range (XeCl 308nm, KrF 248nm, ArF 193nm etc)	Visible (532nm, Green)
A-Si absorption coefficient (cm ⁻¹)	10 ⁶	10 ⁵
Power stability	\pm 10%	\pm 1%
Process ambient	Vacuum/Air	Vacuum/Air, N ₂ , O ₂
Growth mechanism	Random nucleation and growth	Continuous lateral crystallization
Cost (facility maintenance)	High	Low

Table 3-1 The characteristic of the laser beam. The laser power is 3.2W and the scanning speed is 40mm/s.

	Center region	Transition region	Edge region	A-Si region
FWHM (cm-1)	4.97	5.66	17.00	86.46
peak position (cm-1)	513.93	513.32	507.17	484.43
Grain shape	Longitudinal grain	Polygon grain	Circle grain	-----
Grain size	~ 5um*100 um	~ 1um*1 um	~50 nm* 50 nm	-----
Crystallization Mechanism	Longitudinal growth	Partial Melting Growth to SLG-like	SPC	Non-reaction

Table 3-2 The FWHM and peak position of the Raman spectrum with various laser energies at the scanning speed of 50mm/s and the overlapping ratio of 90%.

Laser Energy	2.4W	2.8W	3.2W	a-Si	Si wafer
FWHM (cm-1)	6.25	5.25	5.11	86.46	4.32
Peak position(cm-1)	513.93	513.93	513.93	484.43	520.08

Table 3-3 The FWHM and peak position of the Raman spectrum with various scanning speeds at the laser power of 3.2W and the overlapping ratio of 90%.

Scan Speed	30mm/s	40mm/s	50mm/s	a-Si	Si wafer
FWHM (cm-1)	4.65	5.28	5.86	86.46	4.32
peak position (cm-1)	513.93	513.93	513.32	484.43	520.08

Table 3-4 The FWHM and peak position of the Raman spectrum with various overlapping ratio at the laser power of 3.2W and the scanning speed of 40mm/s.

Overlapping Ratio	90%	80%	70%	60%	50%	a-Si	Si wafer
FWHM (cm-1)	4.93	5.27	5.28	6.19	6.35	86.46	4.32
peak position (cm-1)	513.93	513.93	513.93	513.31	513.31	484.43	520.08

Table 3-5 The measured electrical characteristics of the n-channel TFT crystallized by DPSS CW laser. The scanning speed is 40mm/s, and the overlapping ratio is 90%.

Laser Power (W)	S.S (V/dec)	V_{th}(V)	On/Off current ratio at V_{ds} = 3 V	Mobility(cm²/V-s)
2	2.72	7.93	2.67E+05	19.4
2.4	1.410	0.296	1.16E+06	86.9
3.2	0.753	-1.17	5.58E+06	281

Table 3-6 The measured electrical characteristics of the n-channel TFT crystallized by DPSS CW laser. The scanning speed is 30mm/s, the laser power is 3.2W and the overlapping ratio is 90%.

	S.S (V/dec)	V_{th}(V)	On/Off current ratio at V_{ds} = 3 V	Mobility(cm²/V-s)
Laser Power =3.2W				
Scanning Speed =30mm/s	1.33	-2.71	3.38E+05	388
Overlapping Ratio = 90%				

Figures

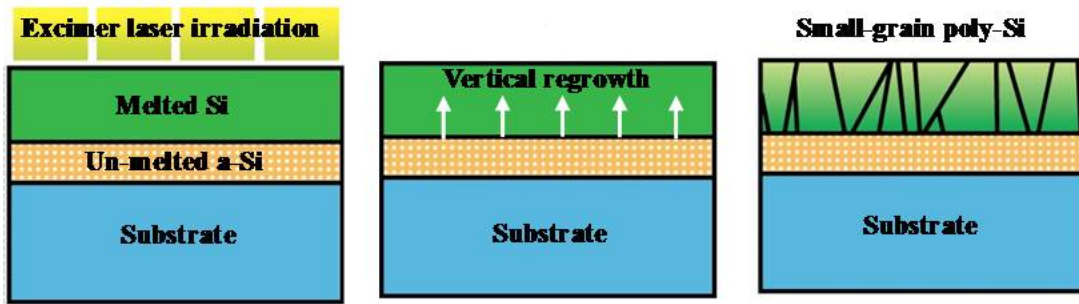


Fig. 1-1 (a) The schematic illustration of the low energy regime corresponding to energy densities that partially melting the a-Si thin film.

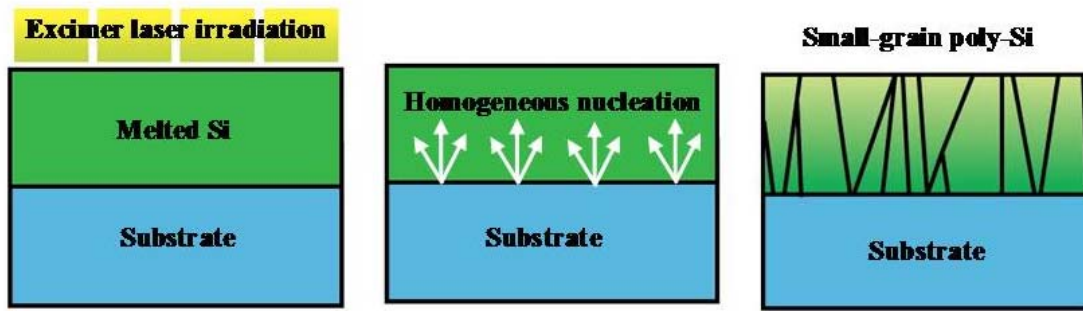


Fig. 1-1 (b) The schematic illustration of the high energy regime corresponding to energy densities that completely melting the a-Si thin film.

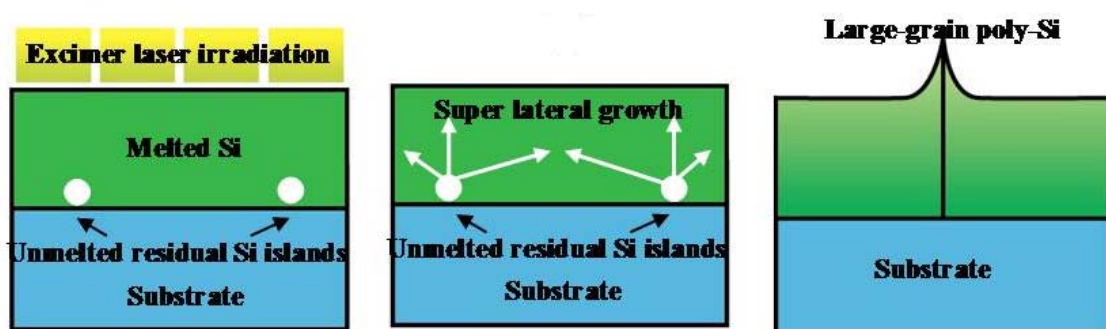


Fig. 1-1 (c) The schematic illustration of the super lateral growth regime corresponding to energy densities that nearly completely melting the a-Si thin film.

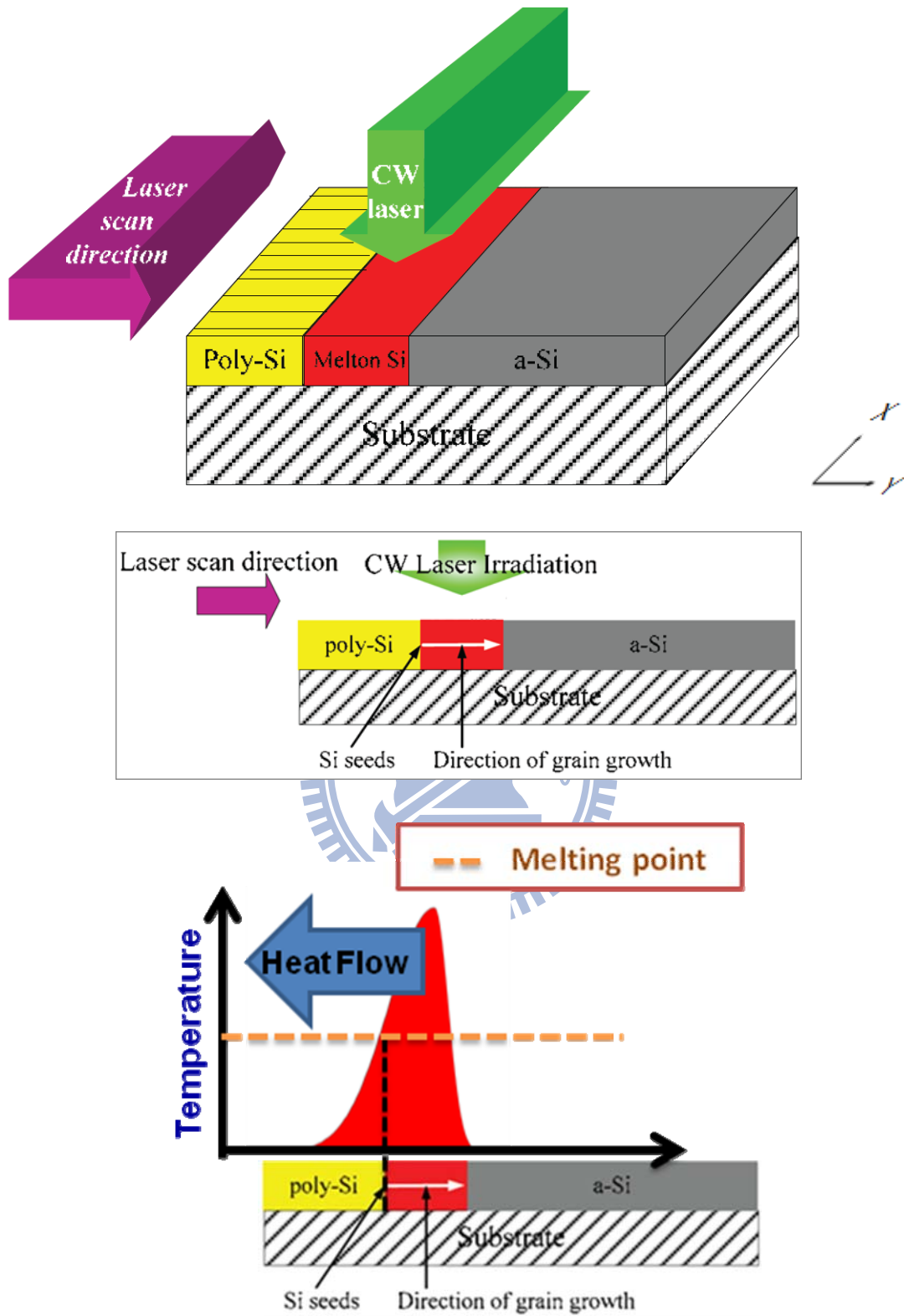


Fig. 2-1 The crystallization mechanism of continuous-wave laser longitudinal grain growth.

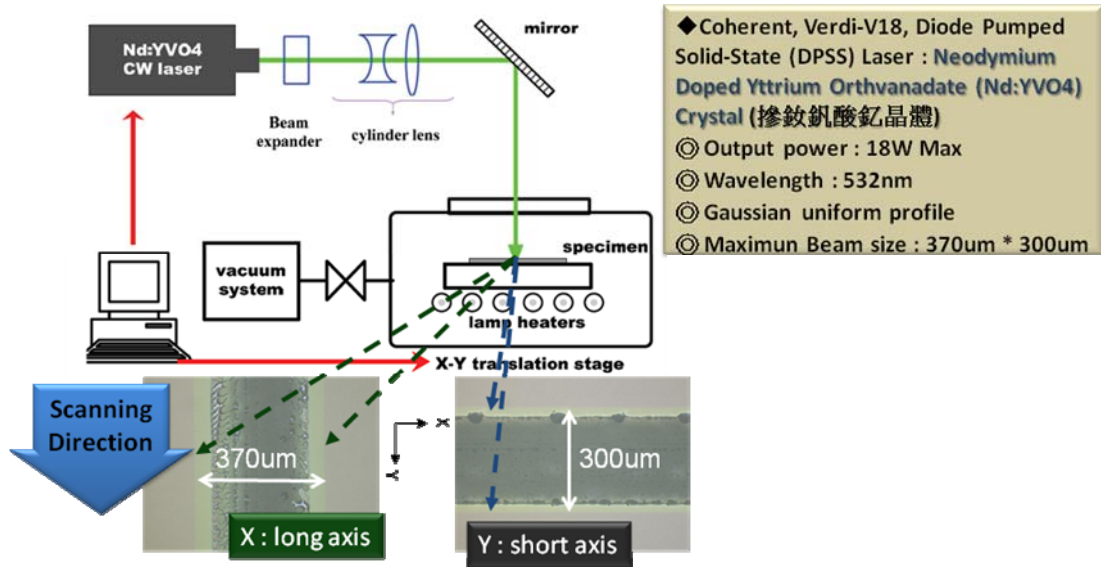
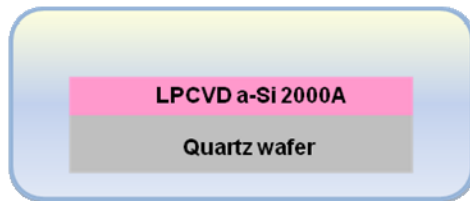
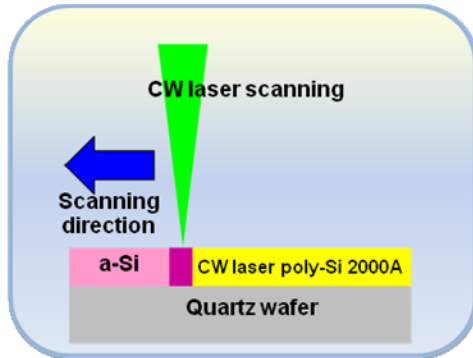


Fig. 2-2 The setup of DPSS continuous-wave laser crystallization.



1

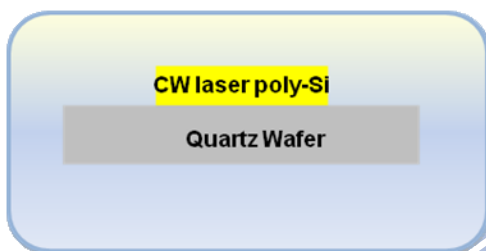
A 2000Å-thick amorphous silicon thin film was deposited by LPCVD at 550 °C on quartz wafer.



2

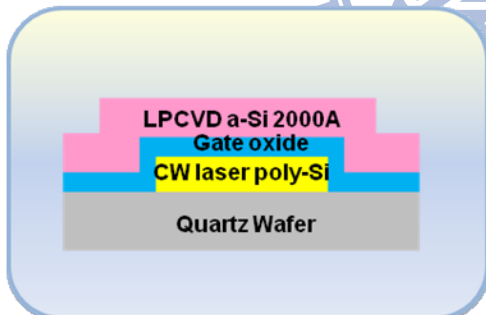
The samples were subjected to CW laser irradiation at room temperature. The laser power, the scanning speed and the overlap ratio were varied :

Laser Power : 1.6W~4.5W
 Laser Scanning Speed : 10mm/s ~ 60mm/s
 Overlapping Ratio : 10%~90%



3

The Active regions were defined by Dielectric Material RIE 200L. (The channel is parallel with the scanning direction.)



4

- a. An 1000Å-thick tetraethyl orthosilicate (TEOS) gate oxide layer was deposited by LPCVD at 700 °C.
- b. A 2000Å-thick a-Si thin film was deposited by LPCVD at 550 °C for gate electrode.

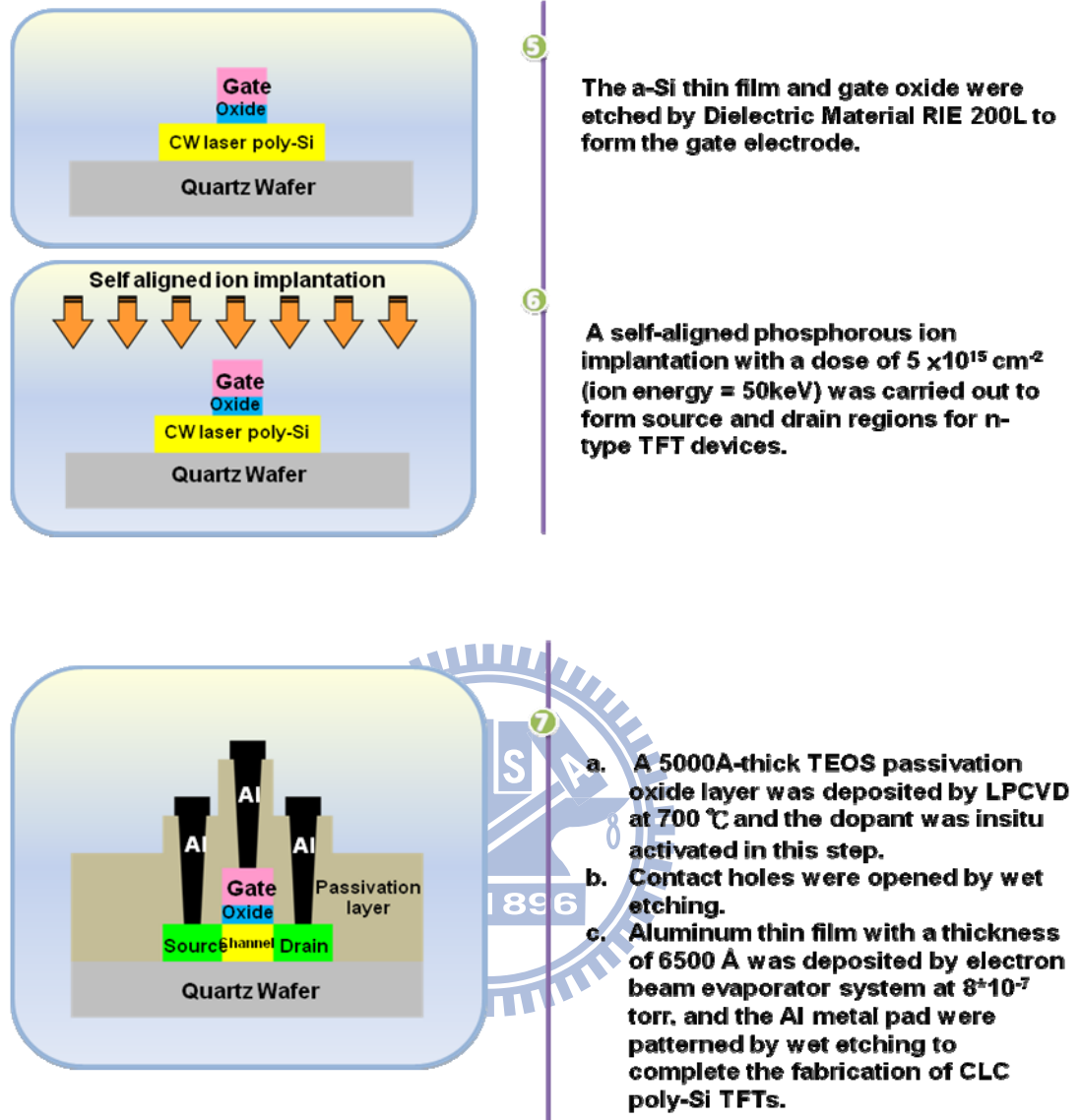


Fig. 2-3 The key process procedures for fabricating CLC TFTs.

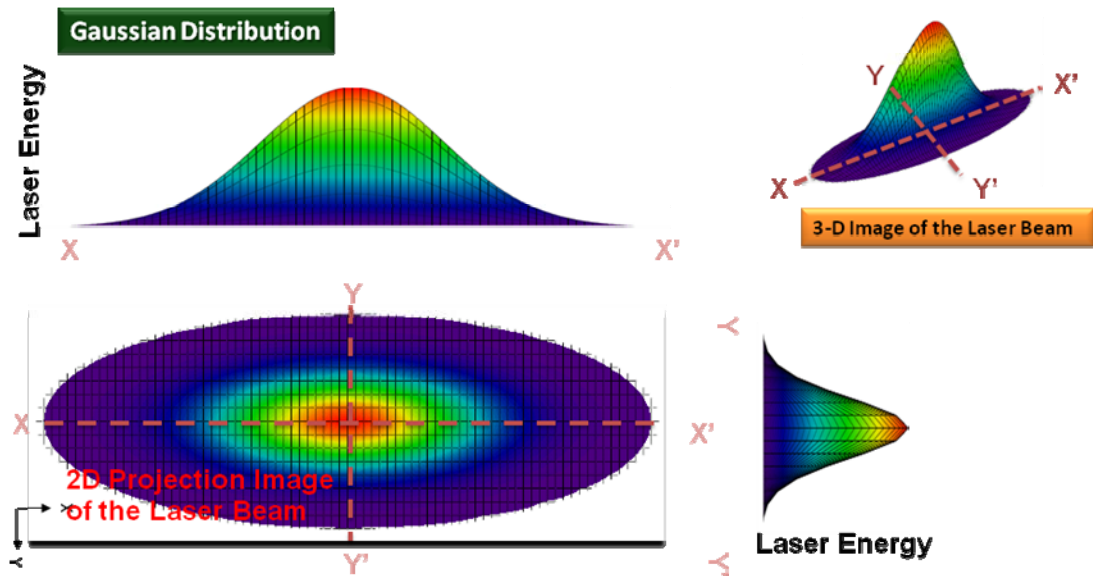


Fig. 3-1 The energy profile of the continuous wave laser beam.

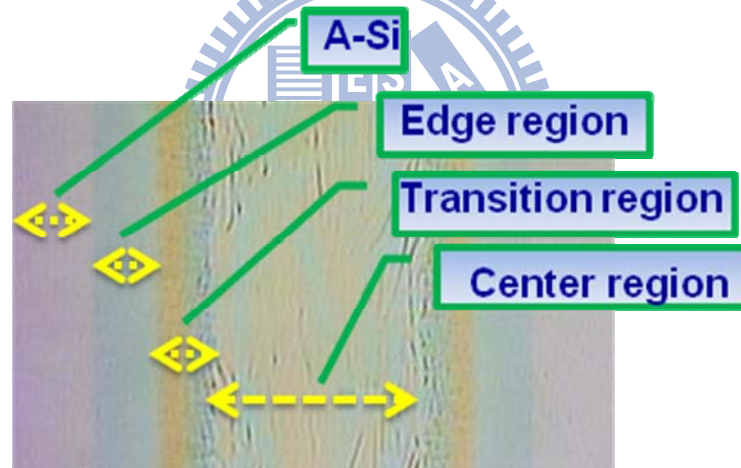


Fig. 3-2 The optical microscopy (OM) image of the laser beam crystallized poly-Si film, the laser power is 3.2W, the laser scanning speed is 40mm/s.

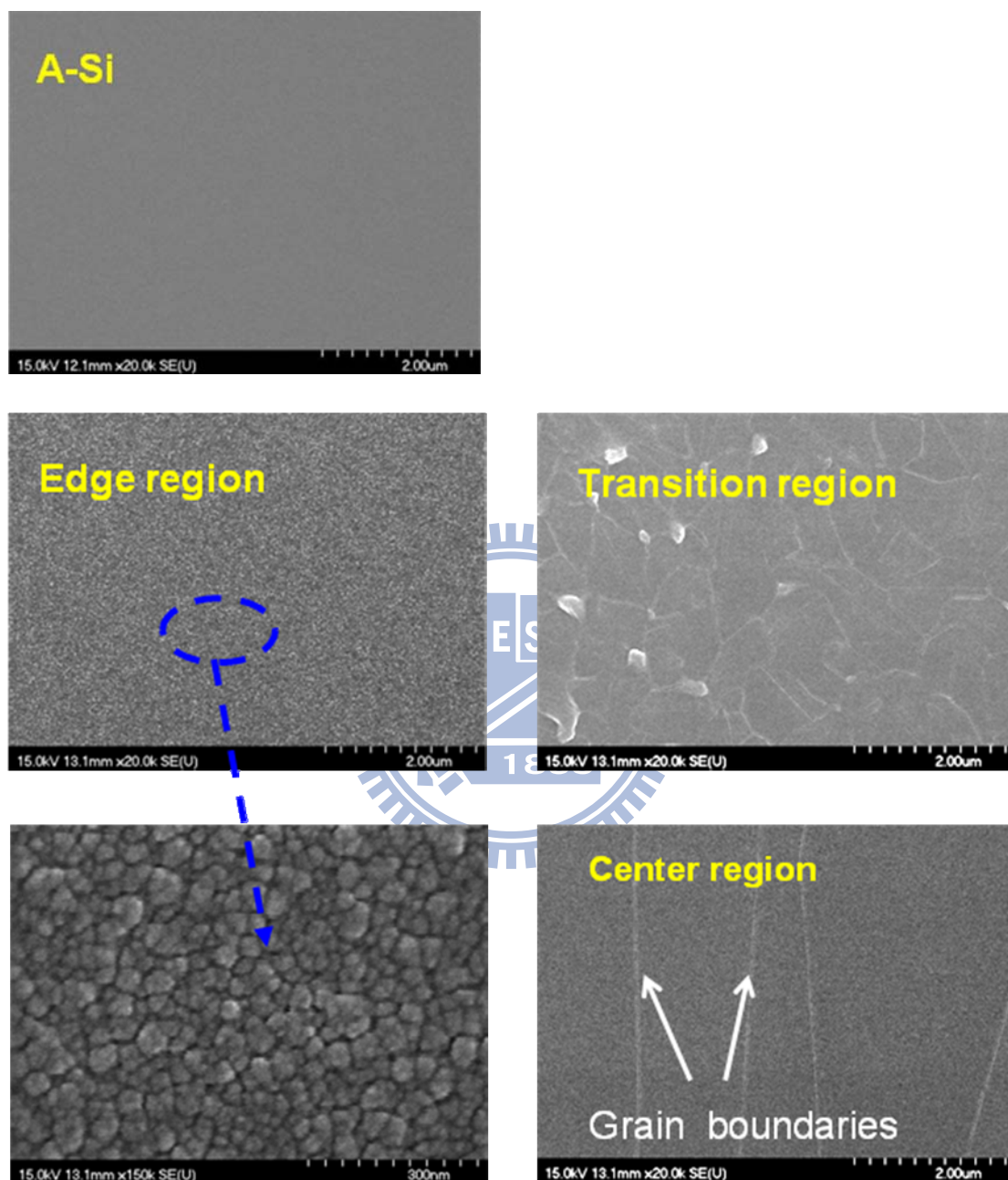


Fig. 3-3 The SEM image of the laser beam, the laser power is 3.2W, and the laser scanning speed is 40mm/s.

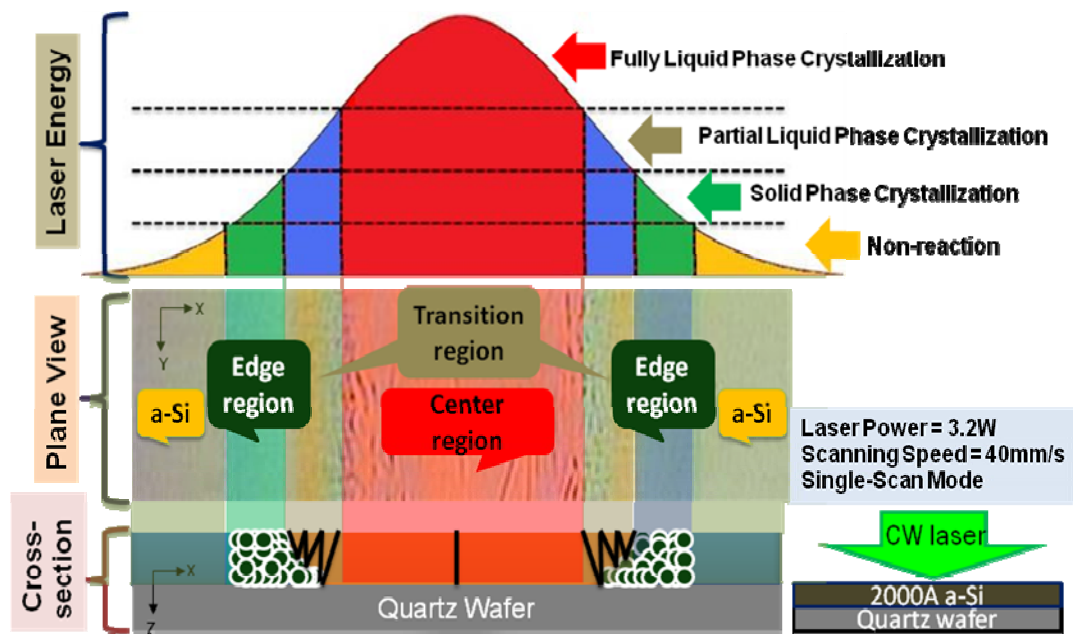


Fig. 3-4 The laser energies in the plane view and cross-section view of the laser beam.

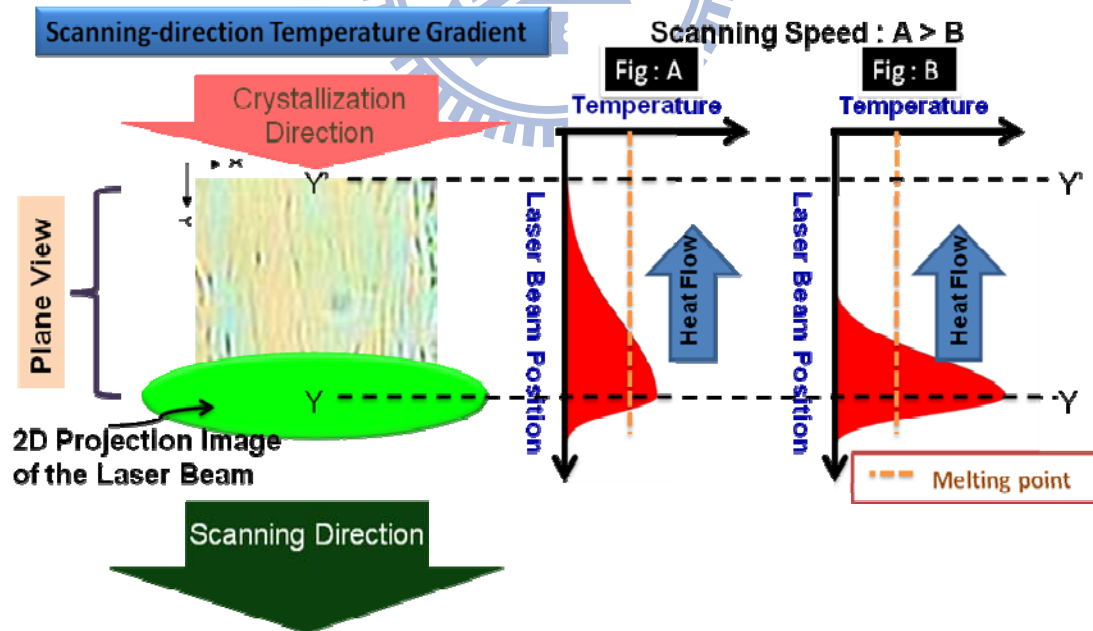


Fig. 3-5 The crystallization mechanism of the longitudinal growth in the center region.

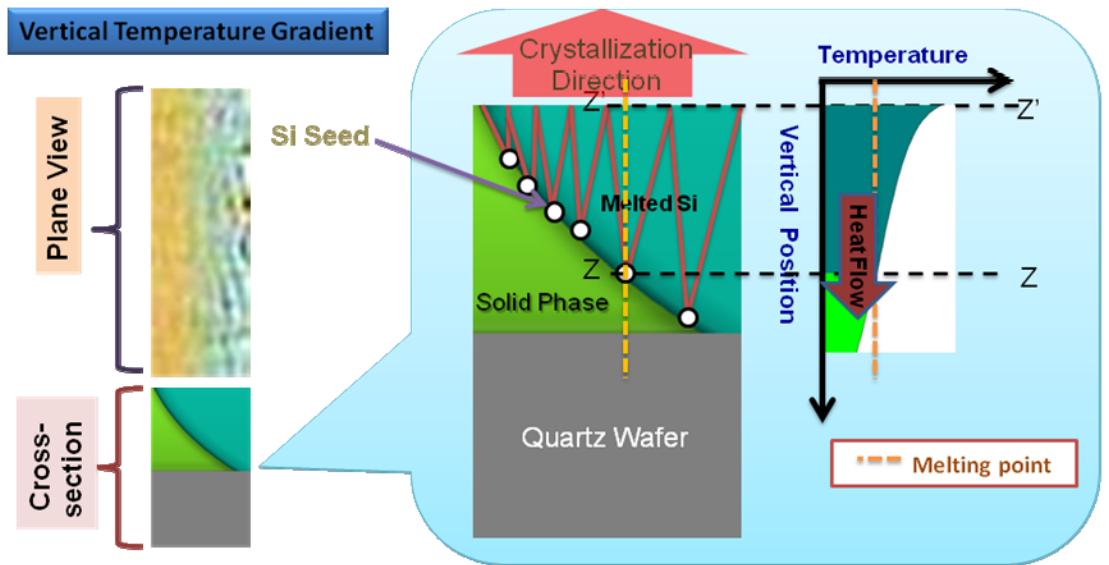


Fig. 3-6 The crystallization mechanism of the PMG to SLG-like in the transition region.

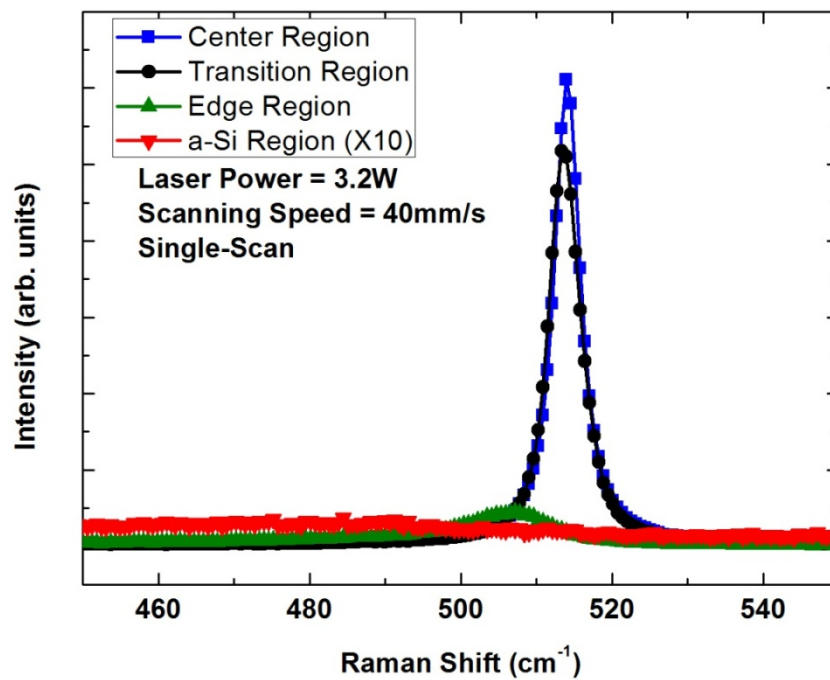


Fig. 3-7 The Raman spectrum of the laser beam.

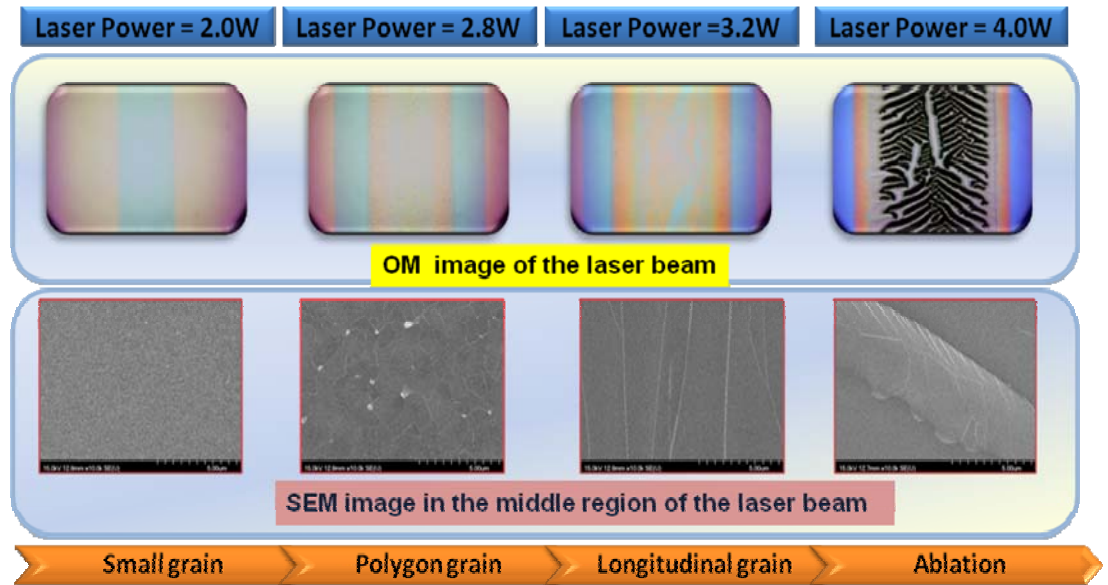


Fig. 3-8 The optical microscopy (OM) and scanning electron microscopy (SEM) images of crystallized poly-Si films with various laser energies at the scanning speed of 50mm/s and single-scan mode, and the laser powers were varied from 2.0W to 4.0W.

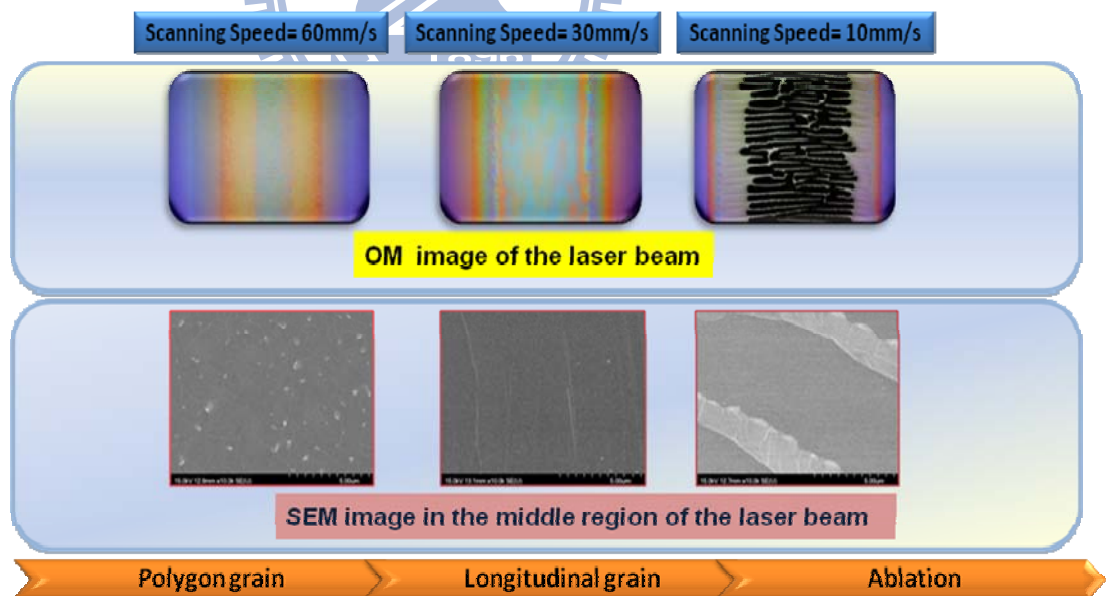


Fig. 3-9 The optical microscopy (OM) and scanning electron microscopy (SEM) images of crystallized poly-Si films with various laser speeds at the laser power of 3W and single-scan mode.

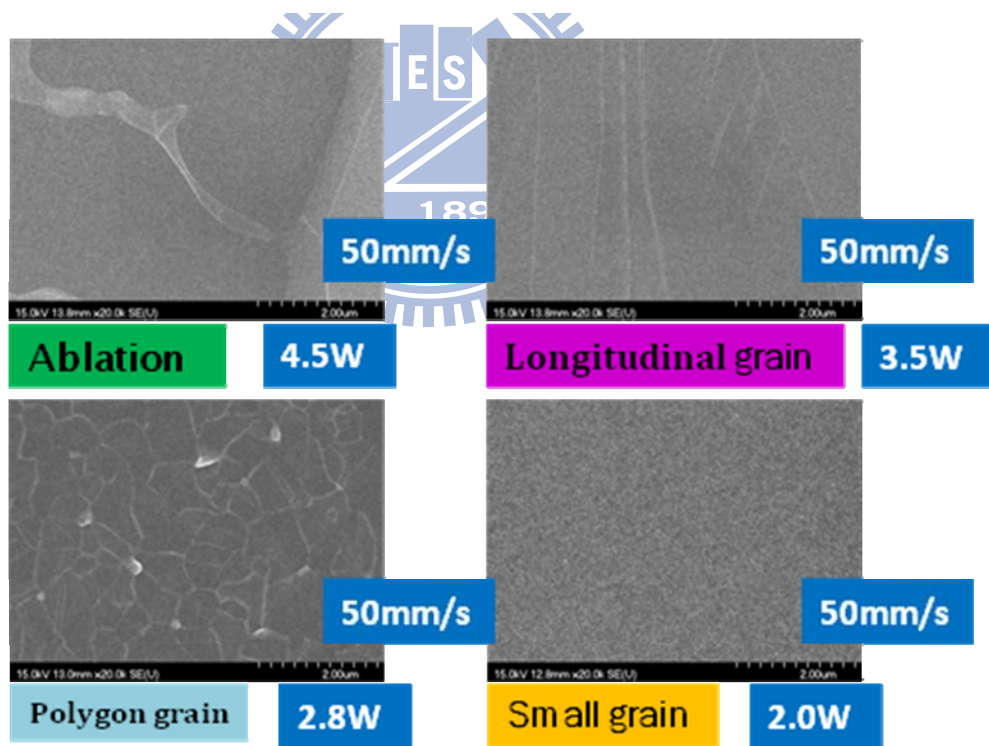
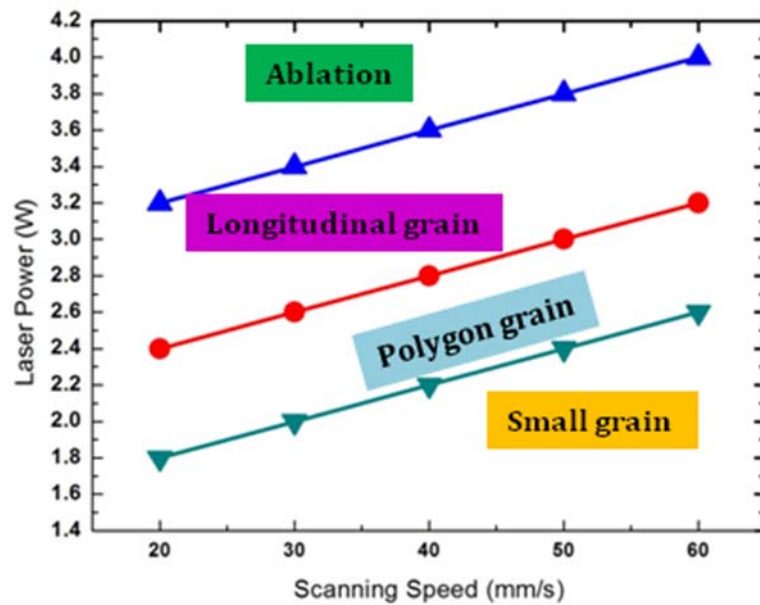


Fig. 3-10 The process window of crystallized poly-Si films at the center region, single-scan mode. Influence of laser power and laser scanning speed on the structure of the grains. The SEM photographs of poly-Si film were crystallized at 2.0W, 2.8W, 3.5W, 4.5W, and the scanning speed is 50mm/s.

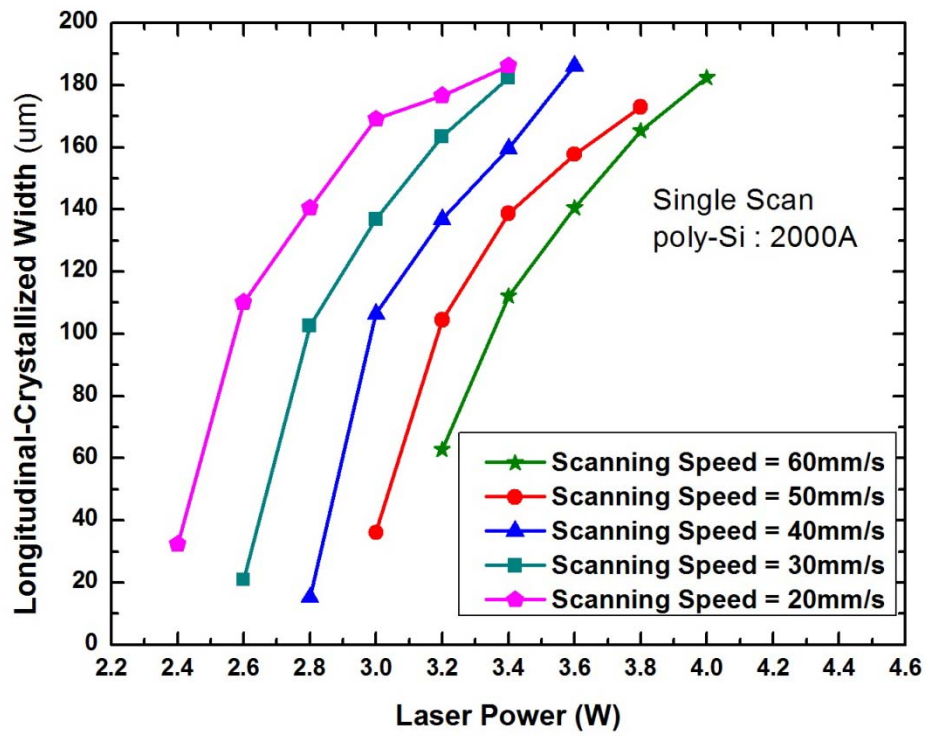


Fig. 3-11 The longitudinal-crystallized widths in the center region of the laser beam.



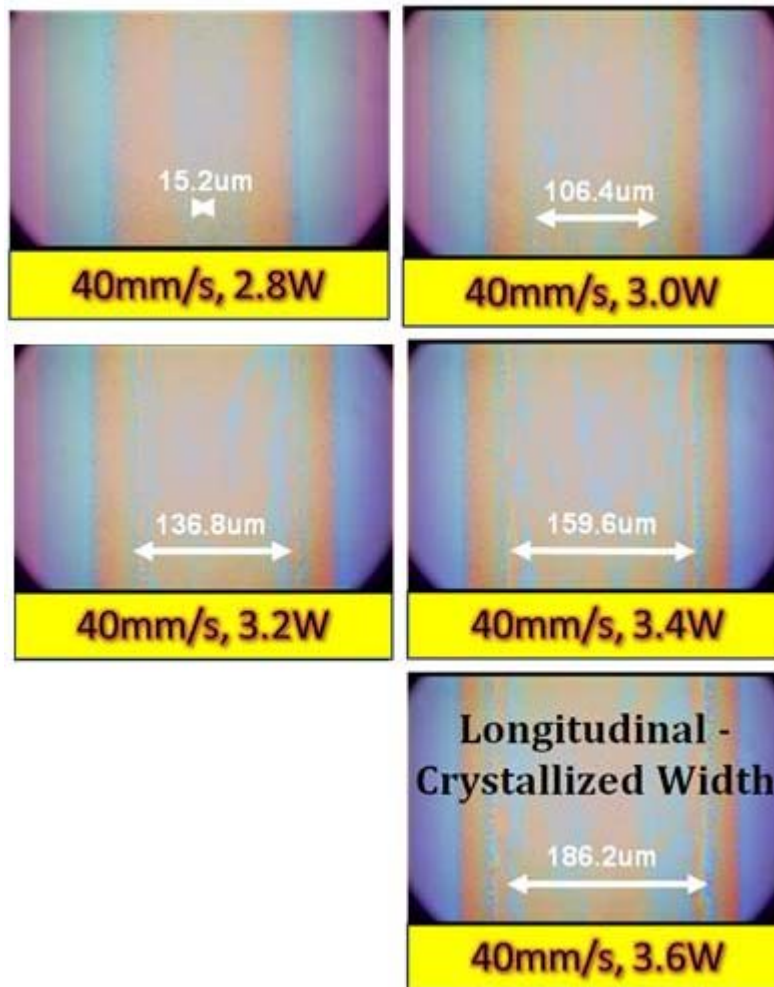


Fig. 3-12 The optical microscopy (OM) images of the longitudinal-crystallized width in the center region of the laser beam.

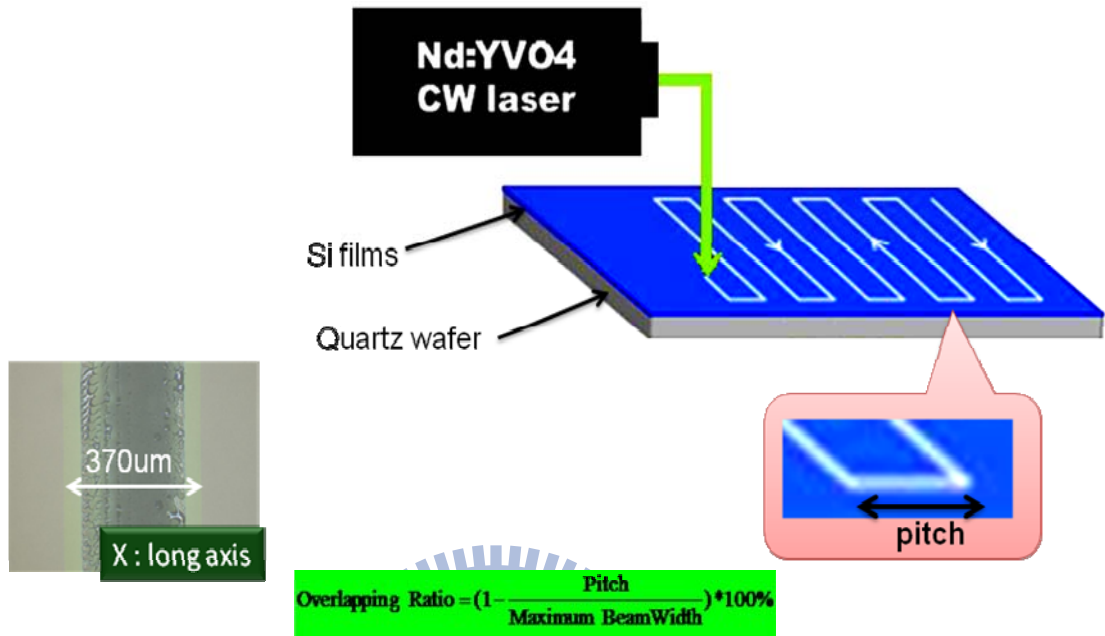


Fig. 3-13 The definition of the overlapping ratio of the laser beam.

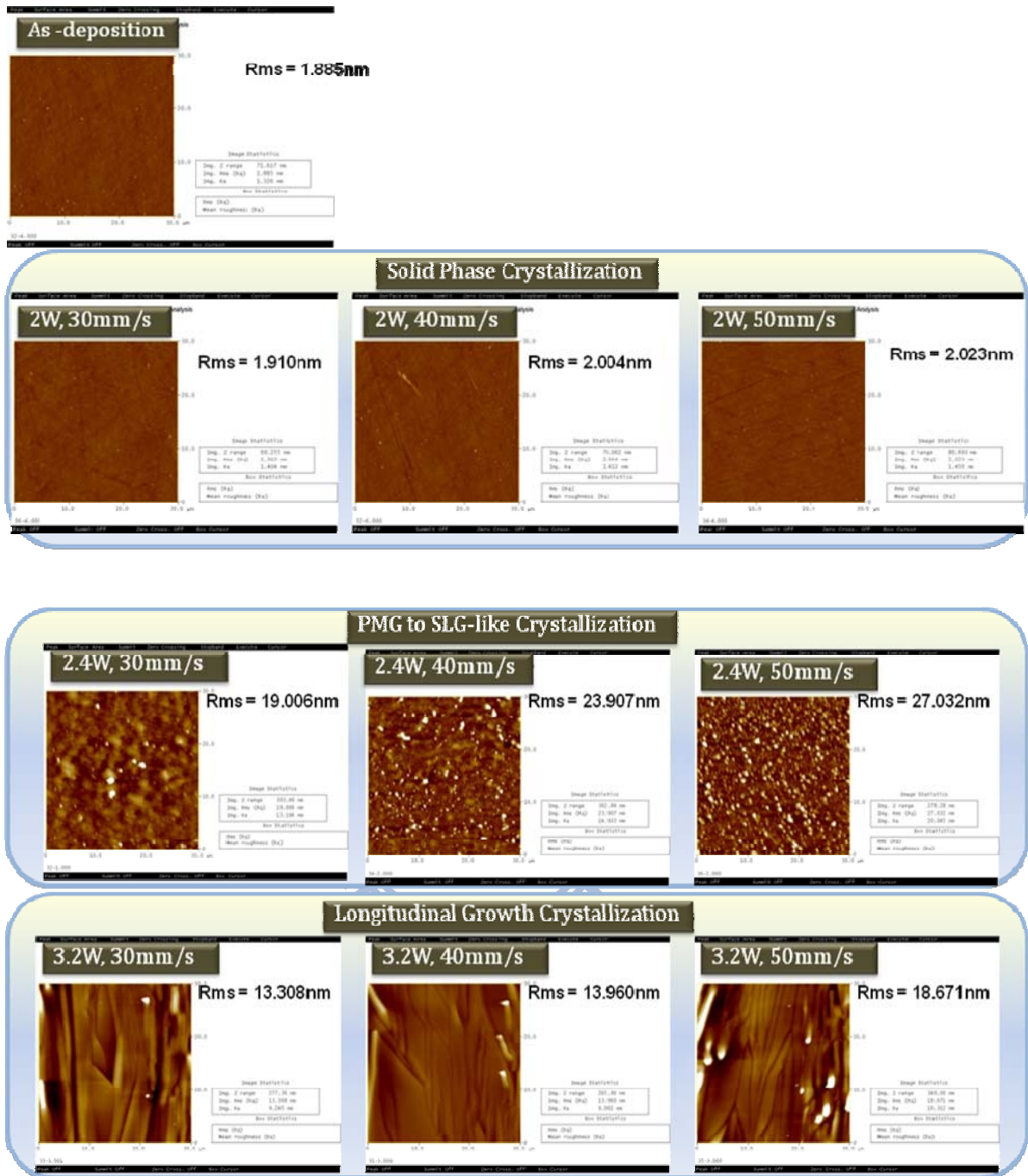


Fig. 3-14 The atomic force microscopy (AFM) images of the crystallized poly-Si films with various laser energies and scanning speeds at the overlapping ratio of 90%.

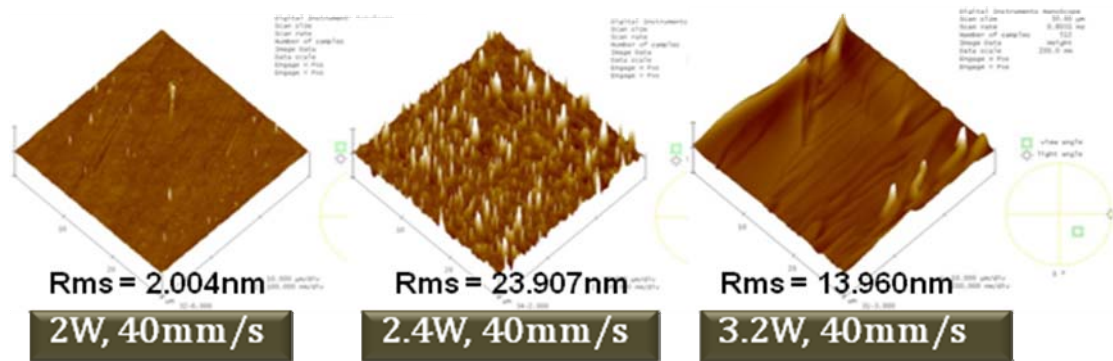


Fig. 3-15 The 3-D images of the crystallized poly-Si films with various laser energies and scanning speeds at the overlapping ratio of 90%.

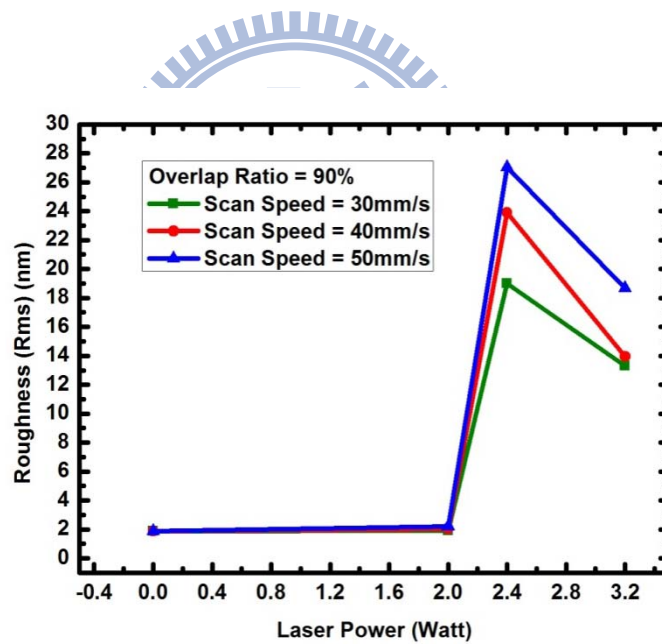


Fig. 3-16 The roughnesses of the crystallized poly-Si films with various laser energies and scanning speeds at the overlapping ratio of 90%.

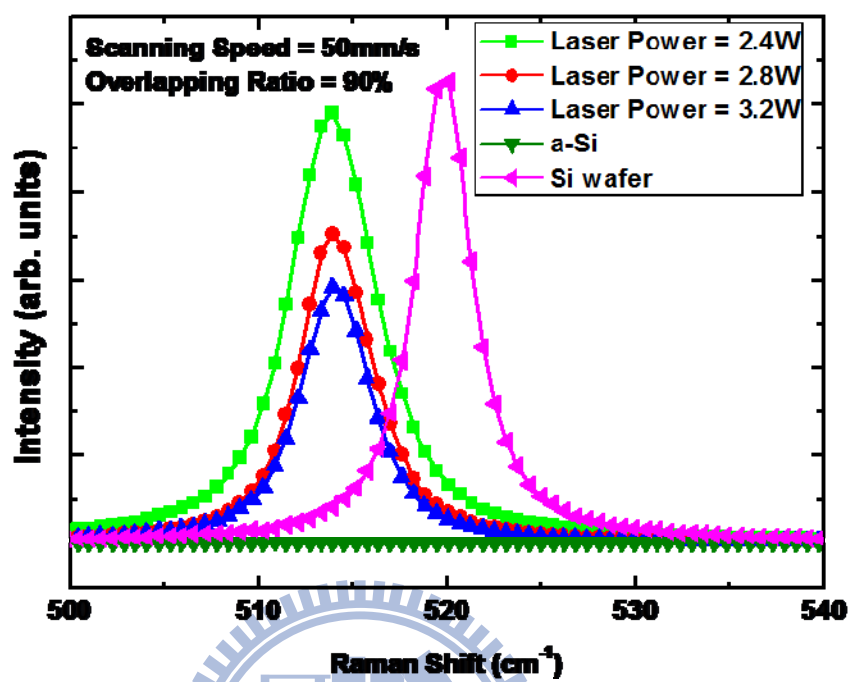


Fig. 3-17 The Raman spectrum of crystallized poly-Si films with various laser energies at the scanning speed of 50mm/s and the overlapping ratio of 90%.

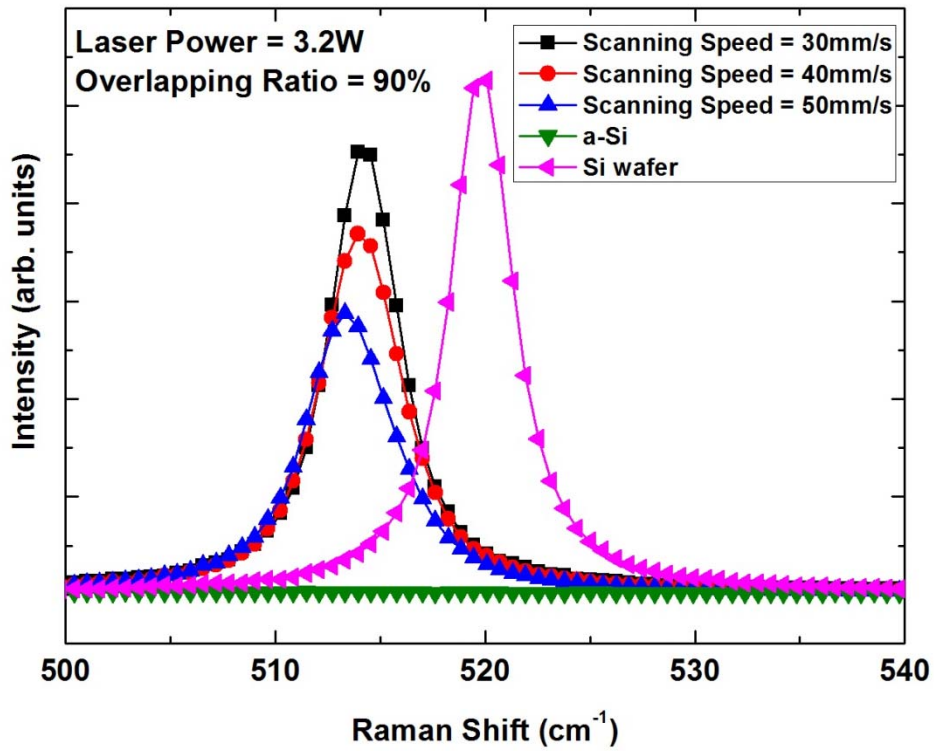


Fig. 3-18 The Raman spectrum of crystallized poly-Si films with various scanning speeds at the laser energy of 3.2W and the overlapping ratio of 90%.

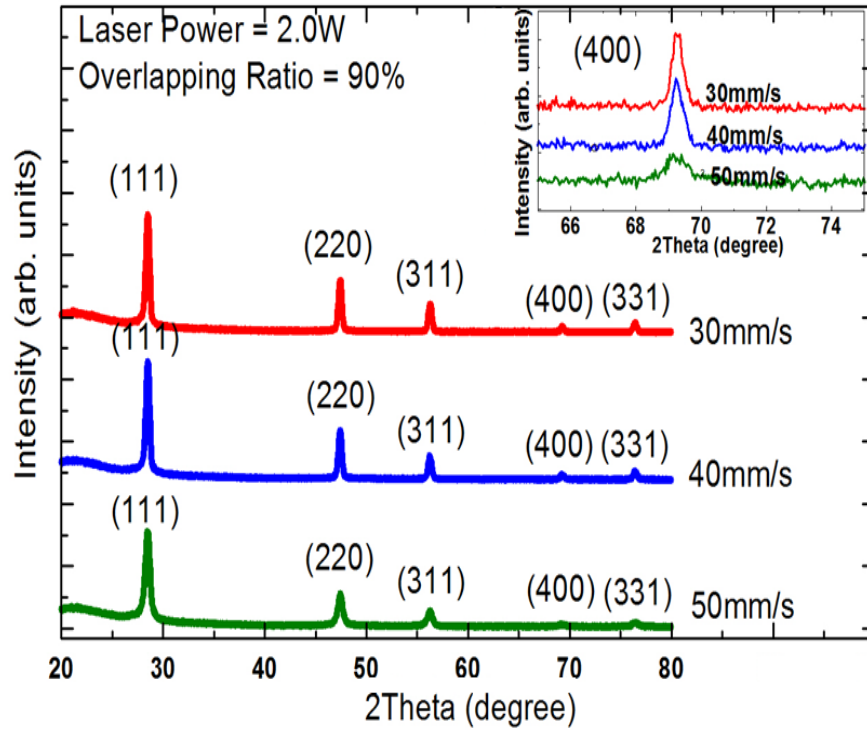


Fig. 3-19 The XRD spectrum of crystallized poly-Si films with various scanning speeds at the laser power of 2W and the overlapping ratio of 90%.

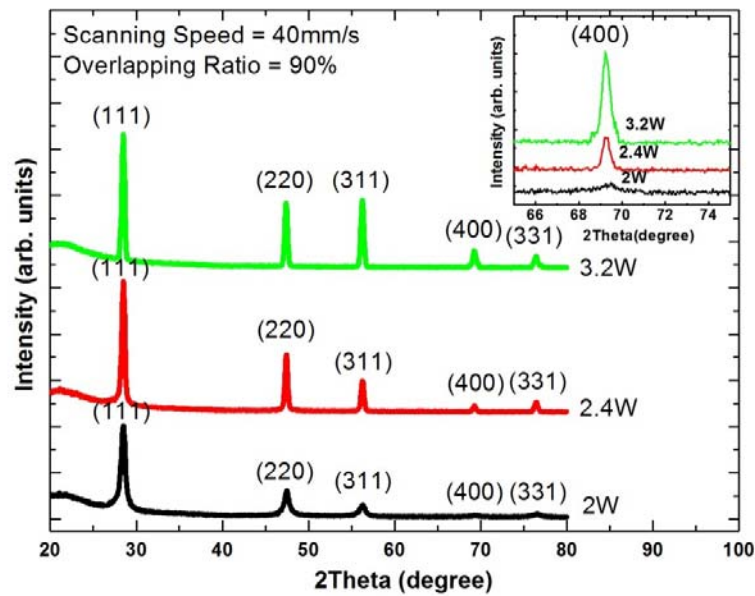


Fig. 3-20 The XRD spectrum of crystallized poly-Si films with various laser powers at the scanning speed of 40mm/s and the overlapping ratio of 90%.

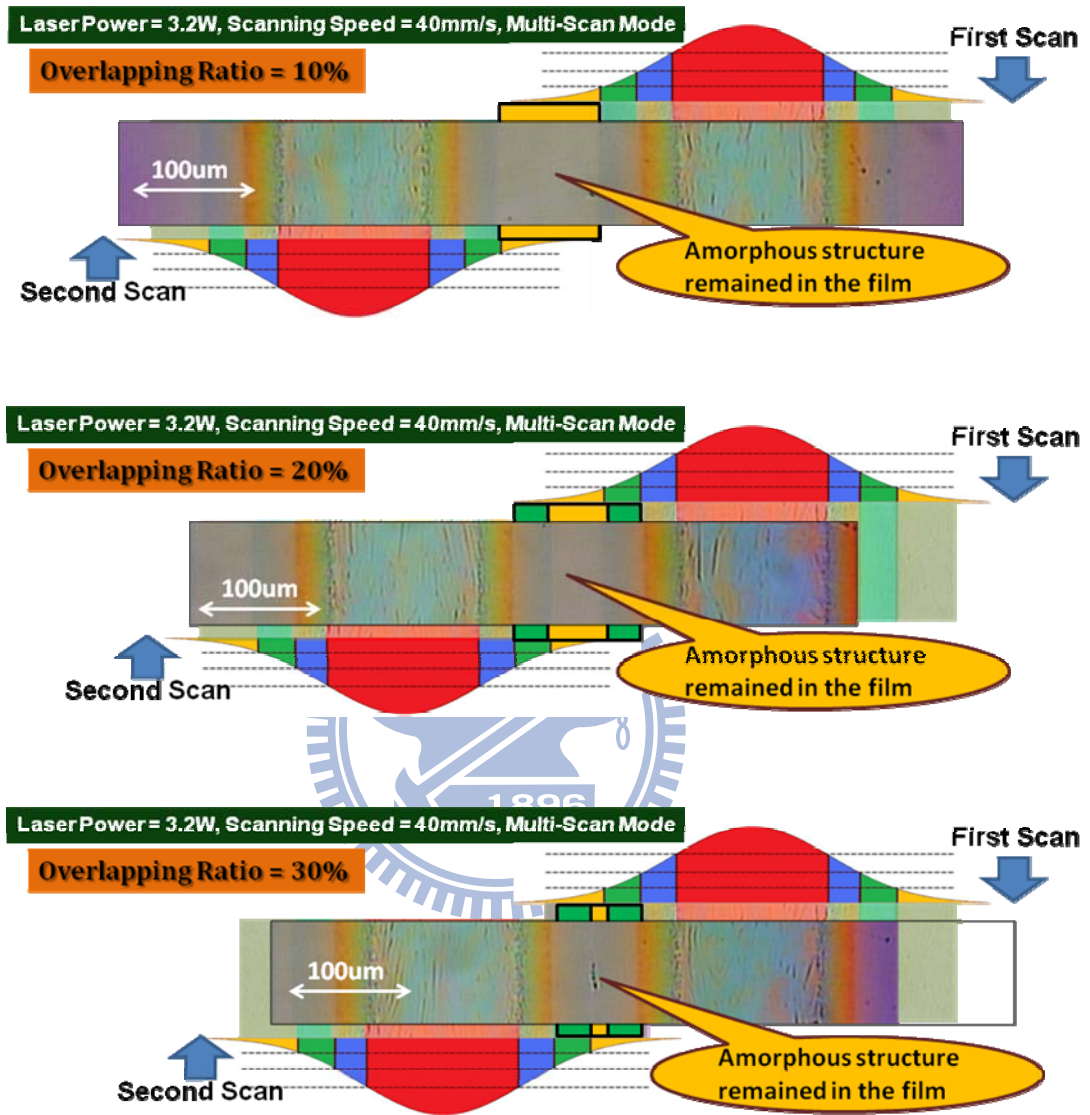
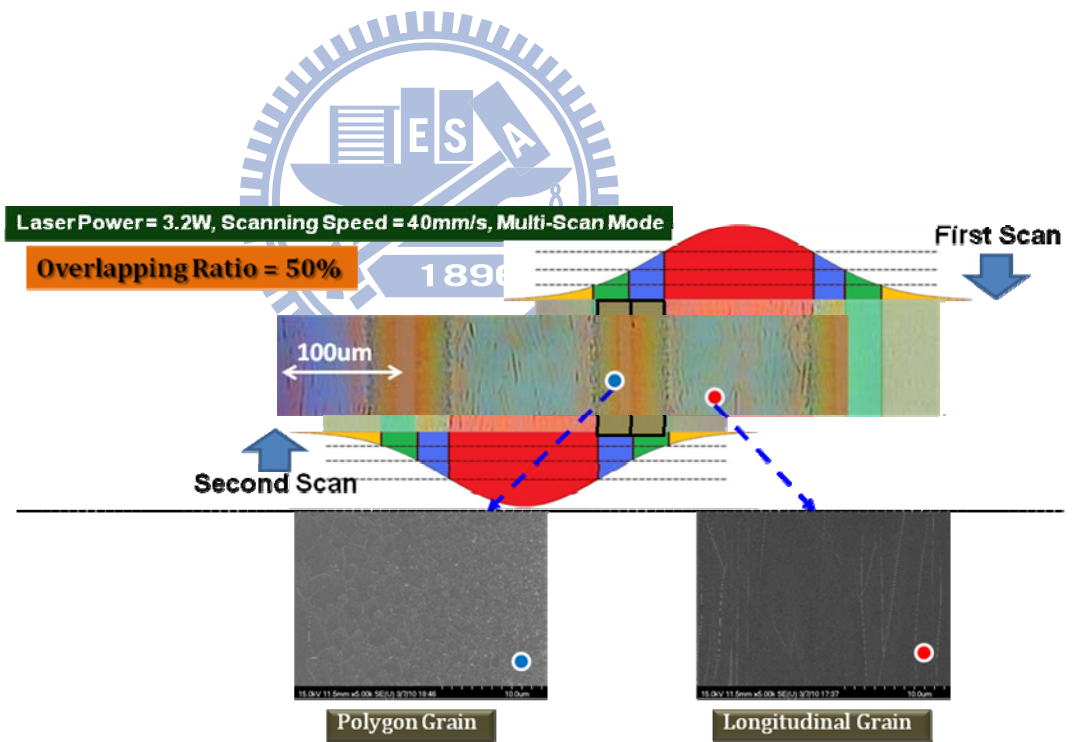
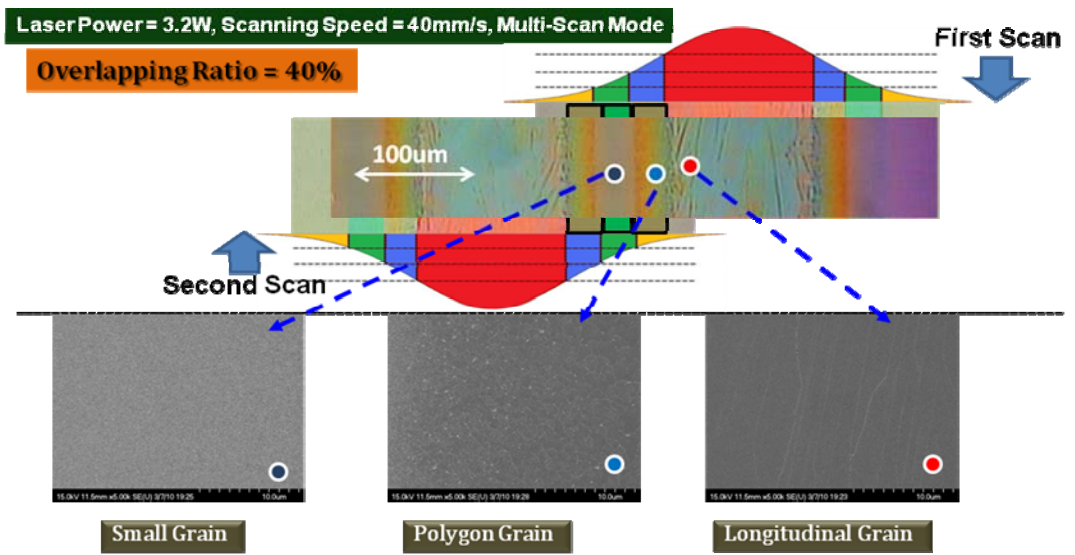


Fig. 3-21 The optical microscopy (OM) images of crystallized poly-Si films with various overlapping ratio from 10% to 30% at the scanning speed of 40mm/s and the laser power of 3.2W.



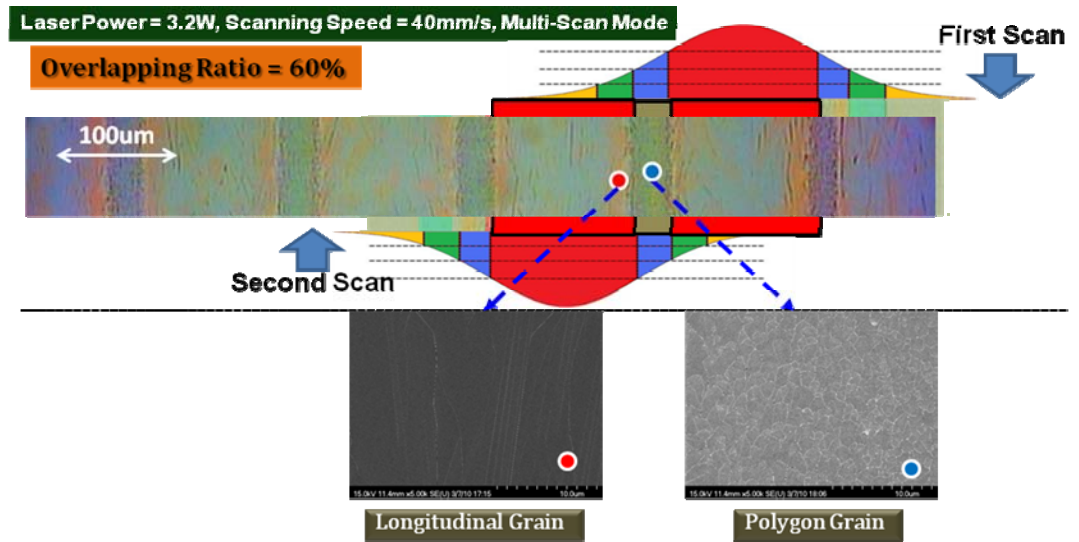
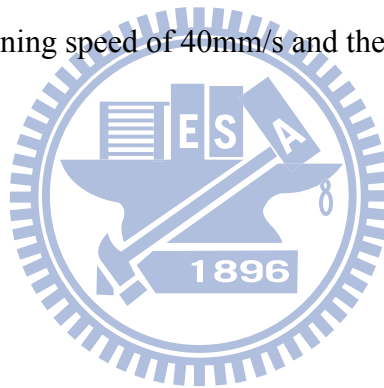
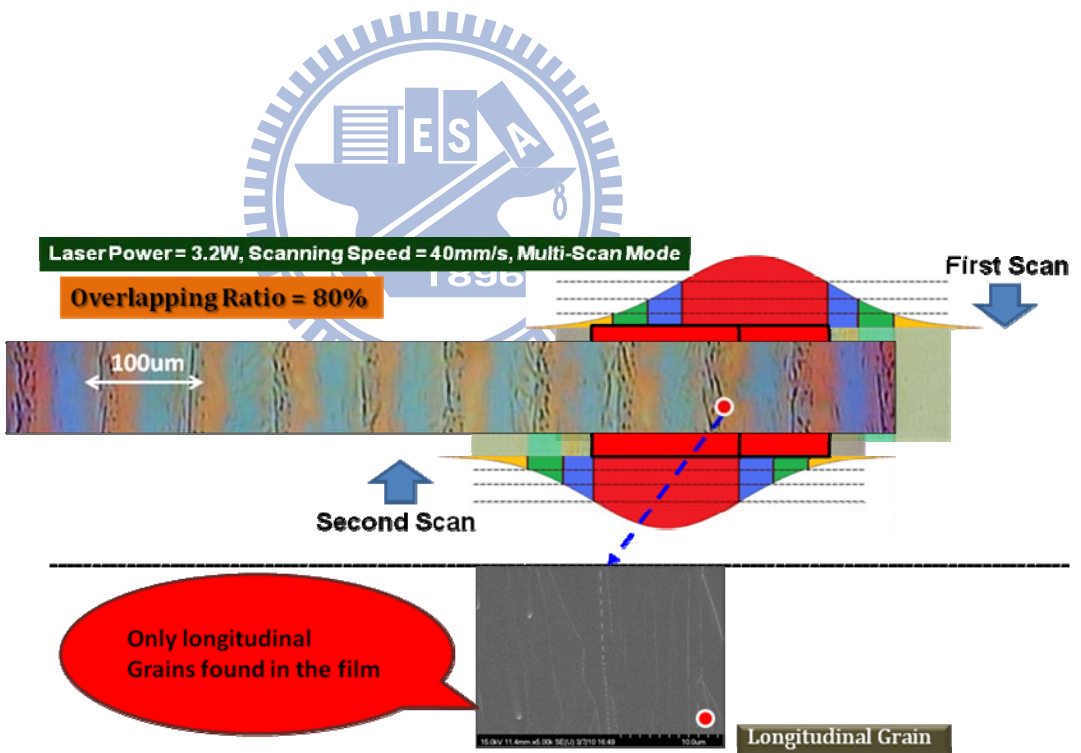
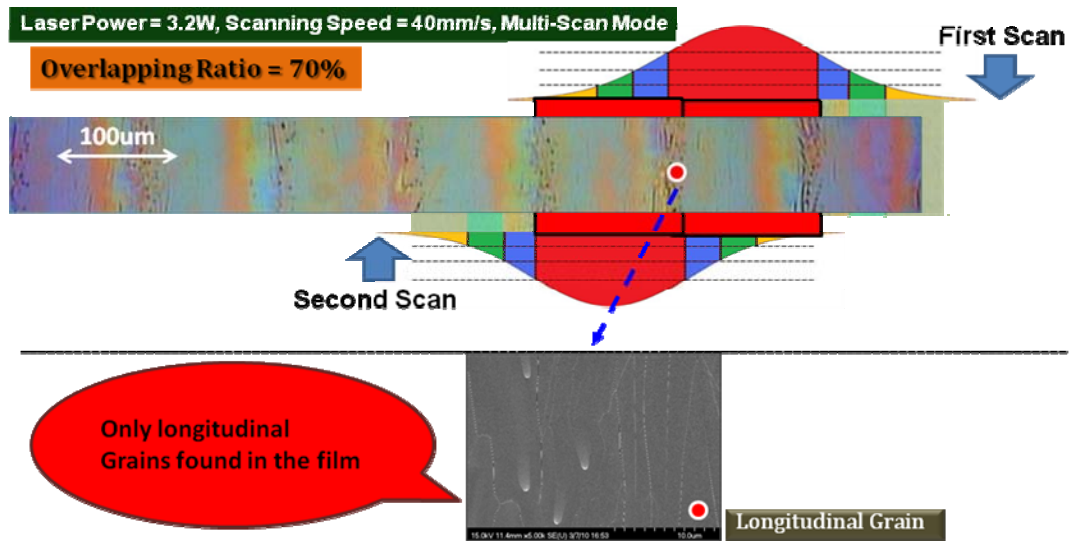


Fig. 3-22 The optical microscopy (OM) and scanning electron microscopy (SEM) images of crystallized poly-Si films with various overlapping ratio from 40% to 60% at the scanning speed of 40mm/s and the laser power of 3.2W.





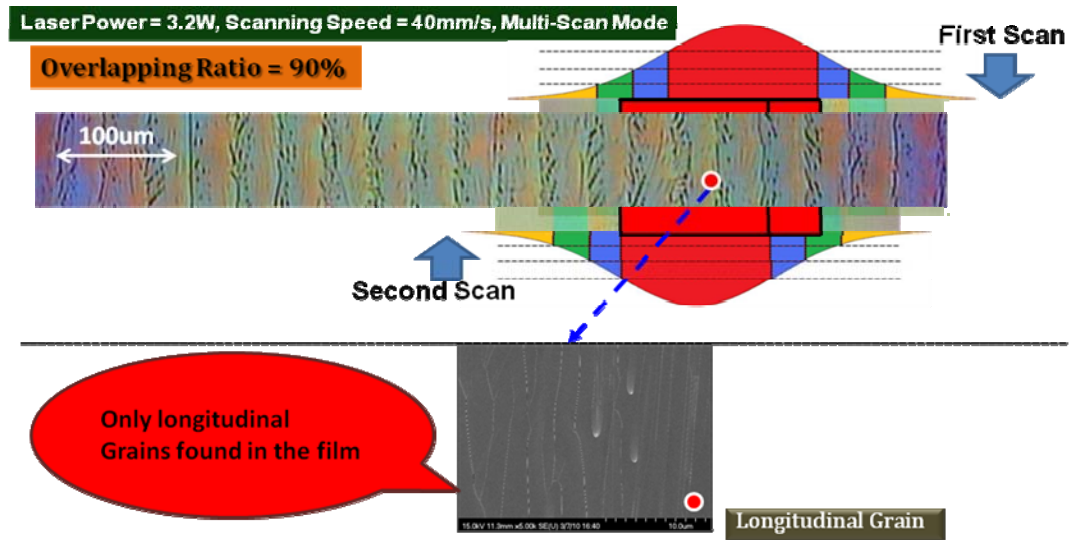


Fig. 3-23 The optical microscopy (OM) and scanning electron microscopy (SEM) images of crystallized poly-Si films with various overlapping ratio from 70% to 90% at the scanning speed of 40mm/s and the laser power of 3.2W.

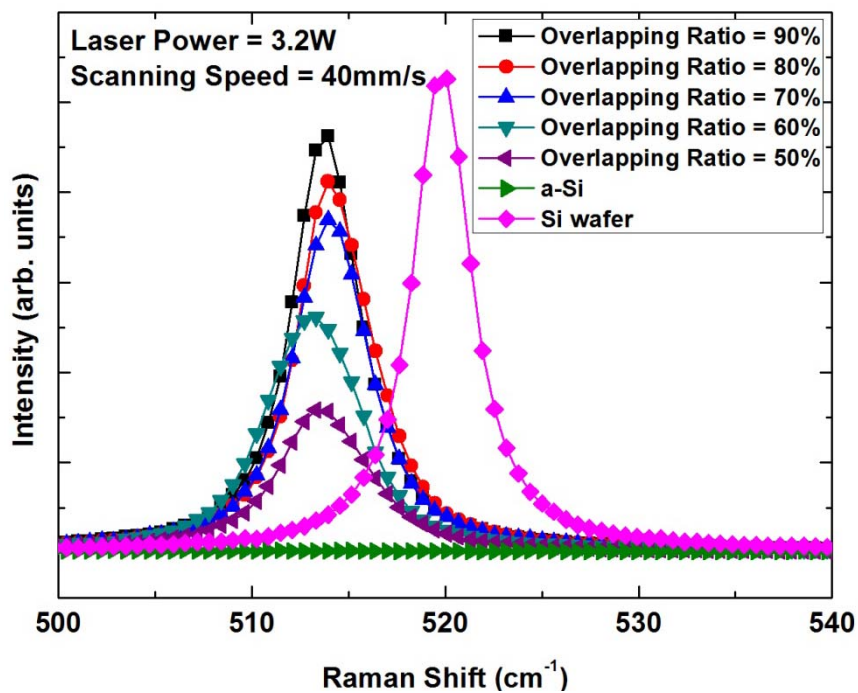


Fig. 3-24 The Raman spectrum of crystallized poly-Si films with various overlapping ratios at the scanning speeds of 40mm/s and the laser power of 3.2W.

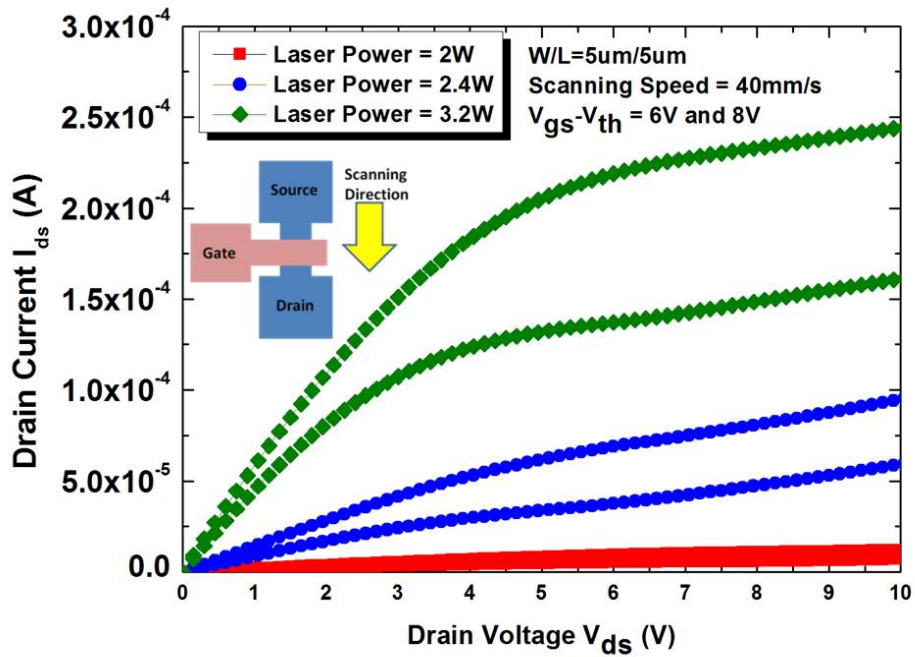
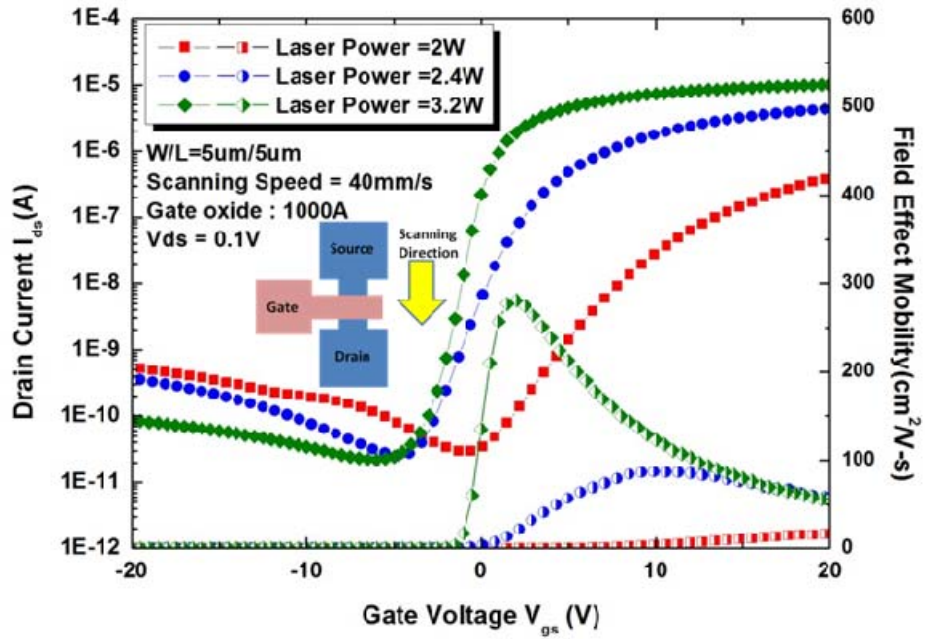


Fig. 3-25 The transfer characteristics and output characteristics of the n-channel TFT crystallized by DPSS CW laser. The scanning speed is 40mm/s, and the overlapping ratio is 90%.

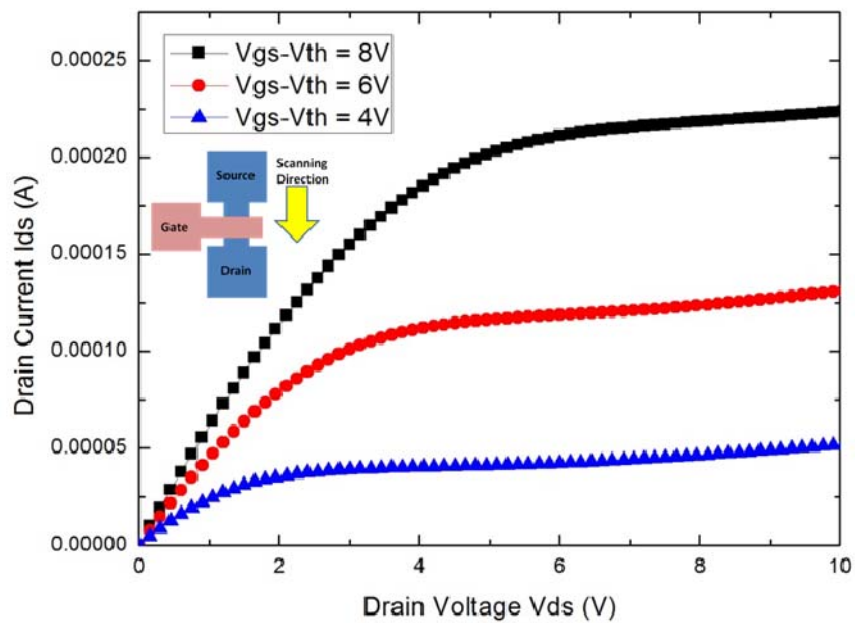
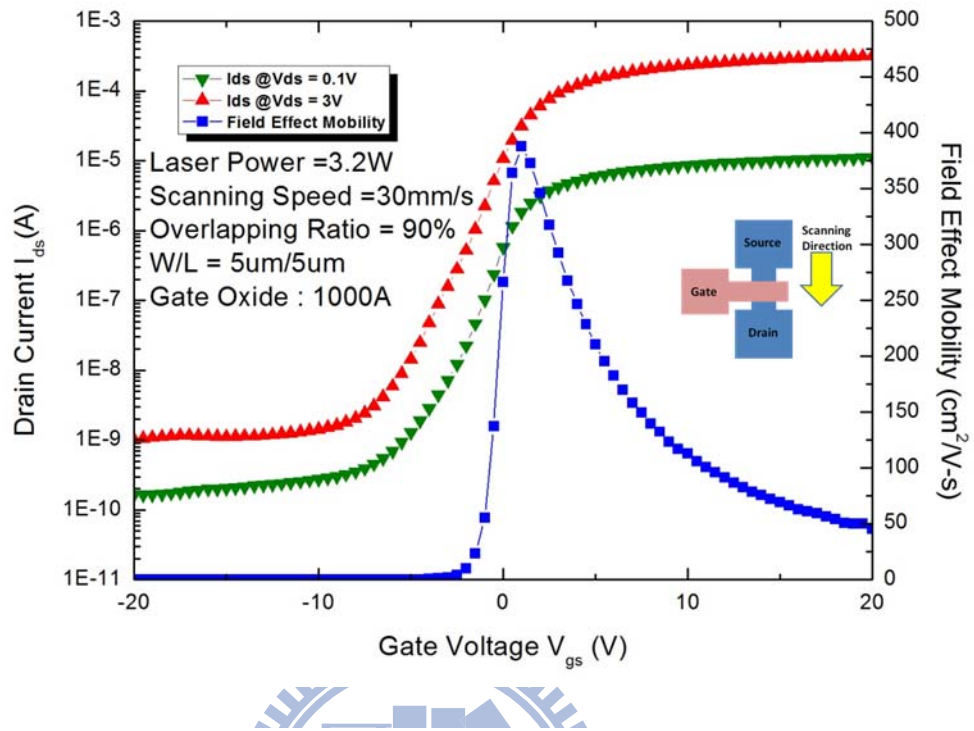


Fig. 3-26 The transfer characteristics and output characteristics of the n-channel TFT crystallized by DPSS CW laser. The scanning speed is 30mm/s, the laser power is 3.2W, and the overlapping ratio is 90%.

References

- [1] S. D. Brotherton, "polycrystalline silicon thin film transistors," *Semi-conduct. Sci. Technol.*, vol. 10, pp. 712-738, 1995
- [2] Yasuhisa Oana, "Current and future technology of low-temperature polycrystalline silicon TFT-LCDs," *Journal of the SID*, vol. 9, pp. 169-172, 2001.
- [3] J. G. Blake, J. D. III Stevens, and R. Young, "Impact of low temperature polycrystalline silicon on the AMLCD market," *Solid State Tech.*, vol. 41, pp. 56-62, 1998.
- [4] Mutsumi Kimura, Ichio Yudasaka, Sadao Kanbe, Hidekazu Kobayashi, Hiroshi Kiguchi, Shun-ichi Seki, Satoru Miyashita, Tatsuya Shimoda, Tokuro Ozawa, Kiyofumi Kitawada, Takashi Nakazawa, Wakao Miyazawa, and Hiroyuki Ohshima, "Low-temperature polycrystalline silicon thin-film transistor driving with integrated driver for high-resolution light emitting polymer display," *IEEE Trans. Electron Devices*, vol. 46, pp. 2282-2288, 1999.
- [5] Mark Stewart, Robert S. Howell, Leo Pires, and Miltiadis K. Hatalis, "Polysilicon TFT technology for active matrix OLED displays," *IEEE Trans. Electron Devices*, vol. 48, pp. 845-851, 2001.
- [6] Atsushi Kohno, Toshiyuki Sameshima, Naoki Sano, Mitsunobu Sekiya, and Masaki Hara, "High performance polycrystalline silicon TFTs fabricated using pulsed laser annealing and remote plasma CVD with low temperature processing," *IEEE Trans. Electron Devices*, vol. 42, pp. 251- 257, 1995.
- [7] Jin-Woo Lee; Nae-In Lee; Hoon-Ju Chung; Chul-Hi Han," Improved stability of polycrystalline silicon thin-film transistors under self-heating and high endurance EEPROM cells for systems-on-panel," in *IEDM Tech. Dig.*, pp. 89 265-268,

1998.

- [8] Matsueda, Yojiro; Park, Yong-Sung; Choi, Sang-Moo; Chung, Ho-Kyoon, "Trend of system on panel" Proceedings of the 5th International Meeting on Information Display, pp. 841-844, 2006.
- [9] Wang, Hongmei ;Chan, Mansun; Jagar, Singh; Wang, Yangyuan; Ko, Ping K., "Submicron super TFTs for 3-D VLSI applications" IEEE Electron Device Letters, v 21, n 9, pp. 391-393, 2000.
- [10] G. Fortunato and P. Migliorato, "Determination of gap state density in polycrystalline silicon by field-effect conductance," Appl. Phys. Lett., vol. 49, p. 1025, 1986.
- [11] I. W. Wu, T. Y. Huang, W. B. Jackson, A. G. Lewis, and A. Chiang, "Passivation kinetics of two types of defects in polysilicon TFT by plasma hydrogenation," IEEE Electron Device Lett., vol. 12, p. 181, 1991.
- [12] M. Cao, T. Zhao, K. C. Saraswat, and J. D. Plummer, "Study on hydrogenation of polysilicon thin film transistors by ion implantation," IEEE Trans. Electron Devices, vol. 42, p. 1134, 1995.
- [13] H. C. Cheng, F. S. Wang, and C. Y. Huang, "Effects of NH₃ plasma passivation on n-channel polycrystalline silicon thin-film transistors." IEEE Trans. Electron Devices, vol. 44, p.64, 1997.
- [14] J. D. Bernstein, S. Qin, C. Chan, and T. J. King, "High dose-rate hydrogen passivation of polycrystalline silicon CMOS TFTs by plasma ion implantation," IEEE Trans. Electron Devices, vol. 43, p. 1876, 1996.
- [15] M. K. Hatalis and D. W. Greve, "High-performance thin film transistors in low

- temperature crystallized LPCVD amorphous silicon films,” IEEE Electron Device Lett. vol. 8, p.361, 1987.
- [16] E. Scheid, B. De Mauduit, P. Taurines and D. Bielle-Daspet, “Super large grain polycrystalline silicon obtained from pyrolysis of SiH₆ and annealing,” Jpn. J. Appl. Phys. Part2, vol. 29, p. L2105, 1990.
- [17] K. Nakazawa, “Recrystallization of amorphous silicon films deposited by low-pressure chemical vapor deposition from Si₂H₆ gas,” J. Appl. Phys., vol. 69, p.1703, 1991.
- [18] C. W. Lin, L. J. Cheng, Y. L. Lu, Y. S. Lee, and H. C. Cheng, “High-performance low-temperature poly-Si TFTs crystallized by excimer laser irradiation with recessed-channel structure,” IEEE Electron Device Lett., vol. 22, p.269, 2001.
- [19] Miltiadis K. Hatalis and David W. Greve, “Large grain polycrystalline silicon by low-temperature annealing of low-pressure chemical vapor deposited amorphous silicon films,” J. Appl. Phys., vol. 63, pp. 2260-2266, 1988.
- [20] K. Zellama, P. Germain, S. Squelard, and J. C. Bourgoin, “Crystallization in amorphous silicon,” J. Appl. Phys., vol. 50, pp. 6995-7000, 1979.
- [21] Miltiadis K. Hatalis and David W. Greve, “Large grain polysrystalline silicon by low-temperature annealing of low-pressure chemical vapor deposited amorphous silicon films,” J. Appl. Phys., vol. 63, pp. 2260-2266, 1998.
- [22] R. B. Iverson, and R. Reif., “Recrystallization of amorphized polycrystalline silicon films on SiO₂: Temperature dependence of the crystallization parameters”, J. Appl. Phys., vol. 62, pp. 1675-1681, 1987.
- [23] L. Hultman, A. Robertsson, H. T. G. Hentzell, I. Engström, and P. A. Psaras.

- “Crystallization of amorphous silicon during thin-film gold reaction” J. Appl. Phys., vol. 62, pp. 3647-3655, 1987.
- [24] Soo Young Yoon, Ki Hyung, Chae Ok Kim, Jae Young Oh, and Jin Jang, “Low temperature metal induced crystallization of amorphous silicon using a Ni solution,” J. Appl. Phys., vol. 82, pp. 5865-5867, 1997.
- [25] Seok-Woon Lee, Yoo-Chan Jeon, and Seung-Ki Joo, “Pd induced lateral crystallization of amorphous Si thin films ”, Appl. Phys. Lett., vol. 66, pp.1671-1673, 1995.
- [26] Zhonghe Jin, Gururaj A. Bhat, Milton Yeung, Hoi S. Kwok, and Man Wong, “Nickel Induced crystallization of amorphous silicon thin films,” J. Appl. Phys., vol. 84, pp.194-200, 1998.
- [27] Hansuk Kim, J. Greg Couillard, and Dieter G. Ast, “Kinetic of silicide-induced crystallization of polycrystalline thin-film transistors fabricated from amorphous chemical-vapor deposition silicon” , Appl. Phys. Lett., vol. 72, pp.803-805, 1998.
- [28] Zhonghe Jin, Hoi S. Kwok, and Man Wong, “Performance of thin-film transistors with ultrathin Ni-MILC polycrystalline silicon channel layers ” IEEE Electron Device Lett., vol. 20, pp. 167-169, 1999.
- [29] Zhiguo Meng, Mingxiang Wang, and Man Wong, “High performance low temperature metal-induced unilaterally crystallized polycrystalline silicon thin film transistors for system-on-panel applications,” IEEE Trans. Electron Devices, vol. 47, pp. 404-409, 2000.
- [30] Jin Jang, Jae Young Oh, Sung Ki Kim, Young Jin Choi, Soo Young Yoon, and Chae Ok Kim, “ Electric-field-enhanced crystallization of amorphous silicon,”

Nature, vol. 395, pp. 481-483, 1998.

- [31] Sang-Hyun Park, Peung-Ik Jun, Kyung-Sub Song, Chang-Kyung Kim, and Duck-Kyun Choi, "Field aided lateral crystallization of amorphous silicon thin film", *Jpn. J. Appl. Phys. Part2*, vol. 38, pp. L108-L109, 1999.
- [32] Won Kyu Kwak, Bong Rae Cho, Soo Young Yoon, Seong Jin Park, and Jin Jang, "A high performance thin-film transistor using a low temperature poly-Si by silicide mediated crystallization," *IEEE Electron Device Lett.*, vol. 21, pp. 107-109, 2000.
- [33] Soo Young Yoon, Jae Young Oh, Chae Ok Kim, and Jin Jang, "Low temperature solid phase crystallization of amorphous silicon at 380°C," *J. Appl. Phys.*, vol. 84, pp. 6463-6465, 1998.
- [34] Soo Young Toon, Ki Hyung, Chae Ok Kim, Jae Young Oh, and Jin Jang, "Low temperature metal induced crystallization of amorphous silicon using a Ni solution," *J. appl. Phys. Vol. 82*, pp. 5865-5867, 1997.
- [35] Soo Young, Seong Jin Park, Kyung Ho Kim, and Jin Jang, "Structural and electrical properties of polycrystalline silicon produced by low-temperature Ni silicide mediated crystallization of the amorphous phase," *J. Appl. Phys. vol. 87*, pp. 609-611, 2000.
- [36] P. M. Smith, P. G. Carey, and T. W. Sigmon, "Excimer laser crystallization and doping of silicon films on plastic substrates" *Appl. Phys. Lett.*, vol. 70, pp. 342-344, 1997.
- [37] S. D. Brotherton, D. J. McCulloch, J. P. Gowers, J. R. Ayres, C. A. Fisher, and F. W. Rohlfing, "Excimer laser crystallization of polycrystalline silicon TFTs for AMLCDs," *Mat. Res. Soc. Symp. Proc.*, vol. 621, Q7.1.1-Q7.1.12, 2000.

- [38] N. M. Johnson, D. K. Biegelsen, H. C. Tuan, M. D. Moyer, and L. E. Fennell, "Single-crystal silicon transistors in laser-crystallized thin films on bulk glass," *IEEE Electron Device Lett.*, vol. 3, pp. 369-372, 1982.
- [39] G. J. Willems, J. J. Poortmans, and H. E. Maes, "A semiempirical model for the laser-induced molten zone in the laser recrystallization process," *J. Appl. Phys.*, vol. 62, pp. 3408-3415, 1987.
- [40] H. W. Lam, R. F. Pinizzotto, and A. F. Tasch Jr, "Single Crystal Silicon-on-Oxide by a Scanning CW Laser Induced Lateral Seeding Process," *J. Electrochem Soc.*, vol. 128, pp. 1981-1986, 1981.
- [41] J. P. Colinge, E. Demoulin, D. Bensahel, and G. Auvert, "Use of selective annealing for growing very large grain silicon on insulator films," *Appl. Phys. Lett.*, vol. 41, pp. 346-347, 1982.
- [42] K. Sera, F. Okumura, H. Uchida, S. Itoh, S. Kaneko, and K. Hotta, "High-performance TFTs fabricated by XeCl excimer laser annealing of hydrogenated amorphous-silicon film," *IEEE Trans. Electron Devices*, vol. 36, pp. 2868-2872, 1989.
- [43] Hiroyuki Kuriyama, Seiichi Kiyama, Shigeru Noguchi, Takashi Kuwahara, Satoshi Ishida, Tomoyuki Nohda, Keiichi Sano, Hiroshi Iwata, Hiroshi Kawata, Masato Osumi, Shinya Tsuda, Shoichi Nakano and Yukinori Kuwano, "Enlargement of Poly-Si Film Grain Size by Excimer Laser Annealing and Its Application to High-Performance Poly-Si Thin Film Transistor," *Japanese Journal of Applied Physics.*, vol. 30, No. 12B, pp. 3700-3703, 1991.
- [44] T. Sameshima, S. Usui, and M. Sekiya, "XeCl Excimer laser annealing used in the fabrication of poly-Si TFT's," *IEEE Electron Device Lett.*, vol. 7, pp.

276-278, 1986.

- [45] Akito Hara, Fumiyo Tajeuchi, Michiko Takei, Katsuyuki Suga, Kenichi Yoshino, Mitsuru Chida, Yasuyuki Sano and Nobuo Sasaki, "High-Performance Polycrystalline Continuous Wave Laser Lateral Crystallization," Japanese Journal of Applied Physics., vol. 41, No. 3B, pp. L311-L313 Part 2, 2002.
- [46] James S. Im, H. J. Kim, and Michael O. Thompson, "Phase transformation mechanisms involved on excimer laser crystallization of amorphous silicon films," Appl. Phys. Lett., vol. 63, pp. 1969-1971, 1993.
- [47] James S. Im and H. J. Kim, "On the super lateral growth phenomenon observed in excimer laser-induced crystallization of thin Si films," Appl. Phys. Lett., vol. 64, pp. 2303-2305, 1994.
- [48] M. O. Thompson, G. J. Galvin, J. W. Mayer, P. S. Peercy, J. M. Poate, D. C. Jacobson, A. G. Cullis, and N. G. Chew, "Melting temperature and explosive crystallization of amorphous silicon during pulsed laser irradiation," Phys. Rev. Lett., vol. 52, pp. 2360-2363, 1984.
- [49] S. R. Stiffler, Michael O. Thompson, and P. S. Peercy, "Supercooling and nucleation of silicon after laser melting," Phys. Rev. Lett., vol. 60, pp. 2519-2522, 1988.
- [50] S. R. Stiffler, M. O. Thompson, and P. S. Peercy, "Transient nucleation following pulsed-laser melting of thin silicon films," Phys. Rev. B, vol. 43, pp. 9851-9855, 1991.
- [51] T. Eiumchotchawalit and James S. Im, "The mechanism of excimer laser-induced amorphization of ultra-thin Si films," Mat. Res. Soc. Symp. Proc., vol. 321, pp.725-730, 1994.

- [52] James S. Im and H. J. Kim, Michael O. Thompson, "Phase transformation mechanisms involved on excimer laser crystallization of amorphous silicon films," Appl. Phys. Lett., vol. 63, pp. 1969-1971, 1993.
- [53] James S. Im and H. J. Kim, "On the super lateral growth phenomenon observed in excimer laser-induced crystallization of thin Si films," Appl. Phys Lett., vol. 64, pp.2303-2305, 1994.
- [54] Robert S. Sposili and James S. Im, "Sequential lateral solidification of thin films on SiO₂," Appl. Phys. Lett. vol. 69, pp. 2864-2866, 1996.
- [55] Hiroyuki Ohshima and Marcel Führen, "High-Performance LTPS Technologies for Advanced Mobile Display Applications," in SID Tech. Dig., 2007, pp. 1482-1485.
- [56] Y. Yamamoto, T. Matsuo, and H. Komiya, "CG Silicon Technology and System Integration for Mobile Applications," in SID Tech. Dig., 2006, pp. 1173-1176
- [57] James S. Im, H. J. Kim, and Michael O. Thompson, "Phase transformation mechanisms involved on excimer laser crystallization of amorphous silicon films," Appl. Phys. Lett., vol. 63, pp. 1969-1971, 1993.
- [58] James S. Im and H. J. Kim, "On the super lateral growth phenomenon observed in excimer laser-induced crystallization of thin Si films," Appl. Phys. Lett., vol. 64, pp. 2303-2305, 1994.
- [59] C. F. Cheng, M. C. Poon, C. W. Kok, and Mansun. Chan, "Impact of transistor-to-grain size statistics on large-grained polysilicon TFT characteristics," in IEDM Tech Dig., 2004, pp. 789-792.
- [60] Mutsumi Kimura, Satoshi Inoue, Tatsuya Shimoda, and Tsukasa Eguchi,

“Dependence of polycrystalline silicon thin-film transistor characteristics on the grain-boundary location,” J. Appl. Phys., vol. 89, pp. 596-600, 2001.

- [61] H. J. Kim and James S. Im, “Multiple pulse irradiation effects in excimer laser-induced crystallization of amorphous Si films,” Mat. Res. Soc. Symp. Proc., vol. 321, pp.665-670, 1994.
- [62] Shuntaro Fujii, Shin-Ichiro Kuroki, Koji Kotani, and Takashi Ito, “Enlargement of Crystal Grains in Thin Silicon Films by Continuous-Wave Laser Irradiation,” Japanese Journal of Applied Physics., vol. 46, No. 4B, pp. 2501-2504, 2007.
- [63] S. Yura, A Sono, T. Okamoto, Y. Sato, T. Kojima, J. Nishimae, M. Inoue, and K. Motonami, “Crystallization of amorphous Si films by a pulsed YAG 2 ω green laser for polycrystalline Si TFT fabrication,” in the proceeding of the International Display Manufacture Conference, 2005, pp. 142-145.
- [64] M. Hatano, T. Sato, M. Matsumura, Y. Toyota, M. Tai, M. Ohkura, and T. Miyazawa, “System on glass display with LTPS TFTs formed using SELAX technology” in the proceeding of the 12th International Display Workshops, 2005, pp. 953-956.
- [65] K. Yamazaki, T. Kudo, K. Seike, D. Ichishima and C. G. Jin, “Double-pulsed laser annealing system and polycrystallization with Green DPSS lasers” in AMLCD Tech. Dig., 2002, pp. 149-152.
- [66] A. Hara, Y. Mishima, T. Kakehi, F. Takeuchi, M. Takei, K. Yoshino, K. Suga, M. Chida, and N. Sasaki, “High Performance Poly-Si TFTs on a Glass by a Stable Scanning CW Laser Lateral Crystallization,” in IEDM Tech Dig, pp.747-750, 2001.
- [67] Akito Hara, Michiko Takei, Fumiyo Takeuchi Suga, Kenichi Yoshino, Mitsuru

Chida, Tatsuya Kakehi, Yoshiki Sano, and Nobuo Sasaki, “High Performance Low Temperature Polycrystalline Silicon Thin Film Transistors on Non-alkaline Glass Produced Using Diode Pumped Solid State Continuous Wave Laser Lateral Crystallization”, Japanese Journal of Applied Physics., vol. 43, No. 4A, pp. 1269-1276, 2004.

[68] Yu-Ting Lin, Chih Chen, Jia-Min Shieh, Yao-Jen Lee, Ci-Ling Pan, Ching-Wei Cheng, Jian-Ten Peng, and Chih-Wei Chao, “Trap-state density in continuous-wave laser-crystallized single-grainlike silicon transistors,” Appl. Phys. Lett., vol. 88, pp.23351, 2006.

[69] Shuntaro Fujii, Shin-Ichiro Kuroki, Xiaoli Zhu, Masayuki Numata, Koji Kotani, and Takashi Ito, “Analysis of continuous-wave laser lateral crystallized polycrystalline silicon thin films with large tensile strain,” Japanese Journal of Applied Physics., vol. 47, No, 4, pp.3046-3049, 2008.

[70] Shuntaro Fujii, Shin-Ichiro Kuroki, Koji Kotani, and Takashi Ito, “Enlargement of Crystal Grains in Thin Silicon Films by Continuous-Wave Laser Irradiation,” Japanese Journal of Applied Physics., vol. 46, No. 4B, pp. 2501-2504, 2007.

[71] Yuta Sugawara, Yukiharu Uraoka, Hiroshi Yano, Tomoaki Hatayama, Takashi Fuyuki, and Akio Mimura, “Crystallization of Doubled-Layered Silicon Thin Films by Solid Green Laser Annealing”, Japanese Journal of Applied Physics., vol. 46, No. 8, pp. L164–L166, 2007.

[72] Yuta Sugawara, Yukiharu Uraoka, Hiroshi Yano, Tomoaki Hatayama, Takashi Fuyuki, and Akio Mimura, “Crystallization of Double-Layered Silicon Thin Films by Solid Green Laser Annealing for High-Performance Thin-Film Transistors”, IEEE Electron Device Lett., vol. 28, No. 5, 2007.

簡歷

姓名：胡明哲

性別：男

籍貫：台南縣

生日：民國七十一年五月二十六日

地址：台南縣麻豆鎮新生南路 218 巷 51 號

學歷：台南縣私立黎明中學高中部（86 年 9 月~89 年 6 月）

國立中正大學電機工程學系（89 年 9 月~95 年 6 月）

國立交通大學電子工程研究所碩士班（96 年 9 月~99 年 8 月）

論文題目：**Study on the Continuous Wave Laser Crystallized
Polycrystalline Silicon Thin-Film Transistors for the
System-on-Panel Applications**

應用於系統面板之連續波雷射結晶多晶矽薄膜電晶體
之研究